# Three dimensional characterisation of intervessel pit membranes in angiosperm xylem based on a shrinkage model and gold perfusion

Zhang Ya[1], Carmesin Cora[1], Kaack Lucian[1], Klepsch Matthias M.[1], Kotowska Martyna[1,2], Matei Tabea[1], Schenk H. Jochen[3], Weber Matthias[4], Walther Paul[5], Schmidt Volker[4], Jansen Steven[1]

[1]Institute of Systematic Botany and Ecology, Ulm University, Albert-Einstein-Allee 11, 89081 Ulm, Germany;

[2]Albrecht-von-Haller Institute for Plant Sciences, University of Göttingen, Untere Karspüle 2, 37073 Göttingen, Germany;

[3]Department of Biological Science, California State University Fullerton, 800 N. State College Blvd., CA 92831-3599 Fullerton, USA;

[4]Institute of Stochastics, Ulm University, Helmholtzstraße 18, 89069 Ulm, Germany;

[5]Central Facility for Electron Microscopy, Ulm University, Albert-Einstein-Allee 11, 89081 Ulm, Germany.

Correspondence

Zhang Ya, Institute of Systematic Botany and Ecology, Ulm University, Albert-Einstein-Allee 11, 89081 Ulm, Germany

Email: ya.zhang@uni-ulm.de

Funding information

Deutsche Forschungsgemeinschaft, Grant number 383393940; National Science Foundation, IOS-1754850; Ministerium für Wissenschaft, Forschung und Kunst Baden-Württemberg (Ideenwettbewerb Biotechnologie).

**Abstract**

Pit membranes between xylem vessels play a major role in angiosperm water transport. Yet, their pore characteristics within a three-dimensional (3D) network of cellulose microfibril aggregates remain largely unknown because of technical difficulties in measuring the dimensions at nanoscale and potential artefacts by sample preparation. Here, we applied a modelling approach based on thickness measurements of fresh (i.e., never dried prior to transmission electron microscopy) and fully shrunken pit membranes. Moreover, pit membrane pore sizes were investigated experimentally by perfusion with colloidal gold particles. Based on our shrinkage model, fresh pit membranes showed a ca. 20 nm distance between layers of microfibril aggregates, a very high mean porosity (0.81), low geodesic tortuosity (1.14), and relatively high constrictivity (0.76). Perfusion experiments showed similar pore sizes in fresh samples, with pores well below 50 nm for seven species. Drying, however, caused a largely irreversible, 50% shrinkage of pit membranes, resulting in much smaller pore sizes, and significant changes of pit membrane porosity, geodesic tortuosity, and constrictivity. These findings provide novel insights in the structure

and function of pit membranes as 3D porous media and contribute to our mechanistic understanding of how they affect hydraulic efficiency and safety of xylem tissue.

**Key words**: angiosperm xylem, bordered pit membranes, cellulose fibrils, dehydration, modelling, pore size, porous media

## Introduction

Making its way from roots to leaves in the hollow xylem conduits of a vascular plant, water passes frequently through the nanoporous, fibrillar matrix of openings in the conduit walls, which, taken together, create most of the resistance along the hydraulic pathway (Choat, Cobb, & Jansen, 2008; Sperry, Hacke, & Pittermann, 2006). These so-called pit membranes between conduits are almost certainly a key evolutionary invention that made it possible for plants to transport large quantities of water under negative pressure. Pit membrane structures and functions are difficult to study, because they cannot be observed in intact plants while under negative pressure, and their ultrastructure is typically observed after at least partial dehydration. Yet, to understand their functions, there is a need to study the ultrastructure of pit membranes in more detail, especially with respect to their 3D characteristics.

Xylem pit membranes are located in bordered pit pairs in conduit cell walls and develop from the primary cell wall and an intervening middle lamella of adjacent vessels (Jane, 1956; Sano, Morris, Shimada, Ronse De Craene, & Jansen, 2011). Traditionally, pit membranes are assumed to serve as a capillary safety valve, because the nanoscale pores formed by the cellulose microfibrils in pit membranes may prevent the spreading of air and pathogens between vessels (Choat et al., 2008; Morris, Brodersen, Schwarze, & Jansen, 2016; Zimmermann, 1983; Zimmermann & Brown, 1971). Despite the importance of the pore sizes and their highly variable shapes for the functioning of pit membranes, the ultrastructure of hydrated pit membranes has been explored in only few species (Pesacreta, Groom, & Rials, 2005). Intervessel pit

membranes consist of various layers of non-woven cellulose microfibrils, which typically form larger aggregates (Figure 1; Choat et al., 2008; Jansen, Choat, & Pletsers, 2009; Schenk, Steppe, & Jansen, 2015). Hydrated microfibril aggregates in intervessel pit membranes had diameters estimated to be between 20 and 50 nm based on atomic force microscopy (Pesacreta et al., 2005). The amount of microfibril aggregates and how these are arranged to each other, determine the pore sizes and thickness of pit membranes, and thus account for the hydraulic resistance of pit membranes and embolism resistance of conduits (Choat et al., 2008; Jansen et al., 2009; Lens et al., 2011; Scholz et al., 2013). An interesting correlation has been found between the intervessel pit membrane thickness and environmental distribution of species, with species from xeric environments typically showing thicker pit membranes than species growing in mesic conditions (Jansen et al., 2009, 2018; Klepsch, Lange, Angeles, Mehltreter, & Jansen, 2016; Li et al., 2016). The correlation between drought occurrence and pit membrane thickness is also reflected in a functional link with embolism resistance, suggesting that thicker pit membranes either confer or are a consequence of higher embolism resistance (Lens et al., 2011; Li et al., 2016; Plavcová & Hacke, 2011; Scholz et al., 2013; Schuldt et al., 2016).

Pit membranes are known to play an important role in drought-induced embolism of xylem. According to the air-seeding hypothesis (Choat et al., 2008; Crombie, Hipkins, & Milburn, 1985; Sperry & Tyree, 1988; Zimmermann, 1983), embolism is triggered when the pressure difference between neighbouring vessels exceeds the capillary force of an air-water meniscus in the 3D pathway of a pit membrane pore, causing air

93 to be sucked in via a series of pore constrictions with variable dimensions. This view,
94 however, requires a 3D view of pit membrane pores with multiple constrictions,
95 which is fundamentally different from the oversimplified 2D view of pit membrane
96 pores, with air-seeding occurring through the single, largest pore (Jansen et al., 2018).
97 Moreover, dehydration of a pit membrane can change the density and arrangement of
98 its microfibril aggregates and may cause irreversible shrinkage (Hillabrand, Hacke, &
99 Lieffers, 2016; Li et al., 2016; Zhang, Klepsch, & Jansen, 2017; Kotowska et al., in
100 press). Pit membranes were reported to shrink by 28% when comparing fresh samples
101 (i.e., never dried before preparation for electron microscopy) with non-fresh samples,
102 including frozen, ethanol stored, and dried samples (Li et al., 2016). Large pores up to
103 700 nm (Table 1) in SEM images of pit membranes could be formed because of the
104 rearrangement of microfibril aggregates during sample preparation (Jansen et al.,
105 2009; Sano, 2005; Shane, McCully, & Canny, 2000). This dehydration artefact may
106 explain the very large variation in pit membrane pores as observed under SEM
107 (Harvey & van den Driessche, 1997; Jansen et al., 2009; Hillabrand et al., 2016; Sano,
108 2005). A large variation in pore sizes (82-200 nm) based on air injection was also
109 suggested for *Rhododendron ponticum* (Crombie et al., 1985). However, pore sizes
110 examined in fresh and wet (i.e., never dried) samples of some angiosperms based on
111 perfusion with different particles show a much smaller variation, ranging from 5 to 37
112 nm (Table 1; Choat, Ball, Luly, & Holtum, 2003; Choat, Jansen, Zwieniecki, Smets,
113 & Holbrook, 2004; Jarbeau, Ewers, & Davis, 1995; Williamson & Milburn, 2017;
114 Zhang et al., 2017). Colloidal gold perfusion in fresh samples of seven angiosperm

species also showed pore sizes between 5 and 20 nm (Choat et al., 2003; Choat et al., 2004; Zhang et al., 2017).

Pit membrane pores are complex three-dimensional spaces, with highly variable and geometrically complex pore volumes that are interconnected by bottlenecks (i.e., constrictions between two adjoining pore spaces) (Bhattad, Willson, & Thompson, 2011). Porous media can generally be characterized by their porosity (ε), geodesic tortuosity (τ), and constrictivity (β) (Figure 2). These 3D characteristics are unknown for pit membranes. Pit membrane porosity (i.e., the pore volume fraction in a pit membrane) represents an important characteristic for hydraulic resistance and vulnerability to air-seeding. The geodesic tortuosity (τ, Figure 2b) can be defined as the ratio of the mean shortest flow path length to the thickness of the porous medium (Neumann, Stenzel, Willot, Holzer, & Schmidt, 2019) and quantifies the geometric complexity of pores in pit membranes (Jansen et al., 2018). If the mean shortest flow path length is equal to the thickness of the porous medium, then the tortuosity value is 1.

The constrictivity (β) is an indicator for constrictions occurring in a porous medium (van Brakel & Heertjes, 1974). For a single tube-like pore, this characteristic is traditionally calculated based on the maximum radius $R_{max}$ and the minimum radius $R_{min}$ of bulges and bottlenecks, respectively (Figure 2b; Petersen, 1958). However, $R_{max}$ and $R_{min}$ cannot be applied directly to complex porous media such as pit membranes, where pore spaces do not consist of single, tube-like pores, but geometrically highly complex and variable volumes. Therefore, constrictivity of

fibrous media such as pit membranes is characterised by the radii of hypothetical spheres occupying the pore space in the porous medium, where $R_{max}$ is the maximum radius of (overlapping) spheres that would cover at least 50% of the pore space in a porous medium (Figure 2c), and $R_{min}$ is the maximum radius of spheres that could theoretically move through the pore constrictions in a certain direction to cover at least 50% of the pore space (Figure 2d). Pore space constrictions would prevent larger spheres from moving in this transport direction, resulting in $R_{min} \leq R_{max}$. When the pore space consists of straight, tube-like pores, $R_{min}$ equals $R_{max}$. The constrictivity (β) is calculated as:

$$\beta = (R_{min} / R_{max})^2 . \qquad \text{(Eqn 1)}$$

Hence, a lower constrictivity value indicates that more constrictions occur in the pore space. Determining the constrictivity of pit membranes is important for gas bubble snap-off inside pores (Kovscek & Radke, 1996; Roof, 1970; Jansen et al., 2018).

This study aims to investigate the porous medium characteristics of intervessel pit membranes by applying a modelling approach that is based on comparing the thickness of fresh and completely shrunken pit membranes. This model, which is based on previous research on pit membranes (Schmid & Machado, 1968; Jansen et al., 2009, 2018; Li et al., 2016; Zhang et al., 2017), allowed us to develop a shrinkage model to estimate the mean pore space between microfibril aggregates in fresh, fully hydrated pit membranes and shrunken pit membranes. It is expected that porosity values of pit membranes are relatively high, similar to other fibrillar, non-woven porous media in nature (Shou, Fan, & Ding, 2011). We also hypothesize that porosity,

geodesic tortuosity, and constrictivity show significant differences between fresh and shrunken pit membranes. Moreover, results from our shrinkage model will be tested against estimations of pore size dimensions by applying perfusion experiments with colloidal gold particles of various sizes to both fresh and dried pit membranes. Based on earlier gold perfusion studies (Choat et al., 2003, 2004; Zhang et al., 2017), we speculate that pore diameters are well below 50 nm in fresh, intact pit membranes, but that pores above 50 nm are common in dried samples with shrunken pit membranes. Whether or not pore sizes are related to pit membrane thickness remains unclear, although pit membranes are expected to be thicker in species from xeric environments, while species growing in more mesic conditions show typically thinner pit membranes. Addressing these topics is not only relevant to our understanding of hydraulic efficiency and safety of plants (Gleason et al., 2015), but will also contribute to the long-standing question of how plants are able to transport water under negative pressure (Jansen & Schenk, 2015; Schenk et al., 2017).

## Materials and Methods

### *Plant material*

Pit membrane thickness was examined in fresh petioles and/or stems of ten angiosperm species (Table 2). Most of the species selected were common woody angiosperms growing at Ulm University (e.g., *Acer pseudoplatanus* L., *Alnus glutinosa* (L.) Gaertn., *Corylus avellana* L., *Fagus sylvatica* L., *Populus tremula* L.). An additional number of species was selected to obtain clear differences in pit

181 membrane thickness across the species selected. We therefore added samples of
182 *Hibiscus schizopetalus* (Dyer) Hook.f., *Liriodendron tulipifera* L., *Cinnamomum*
183 *camphora* (L.) J.Presl, *Nerium oleander* L., and *Persea americana* Mill., which were
184 growing at the glasshouses of the botanical garden of Ulm University.

185 Fresh and dried-rehydrated petioles of three species (*A. pseudoplatanus*, *C. camphora*,
186 and *P. americana*) were used to investigate the effect of sample drying on pit
187 membrane pore sizes. The petioles were taken from mature, fully developed leaves.
188 Moreover, colloidal gold perfusion was also applied to fresh stems of *A. glutinosa*, *H.*
189 *schizopetalus*, *N. oleander*, and *P. tremula* (Table 2). The stem material used was 7 to
190 10 mm in diameter, and 2 to 3 years old. One advantage of using petioles for gold
191 perfusion experiments instead of stems is that the vascular bundles in petioles require
192 a smaller amount of colloidal gold for injection. Also, the lower amount of lignified
193 tissue in leaves makes these easier for transmission electron microscopy (TEM)
194 preparation than stems. All stem and petiole samples were collected in the morning
195 during 2016 and 2017, and brought to the laboratory within 15 min.

196 *Intervessel pit membrane thickness measurements*

197 A standard protocol was followed to prepare ultrathin sections for TEM (Jansen et al.,
198 2009; Zhang et al., 2017). Briefly, small cubes of xylem (1 x 2 x 2 mm) from the
199 current growth ring were cut under water, fixed overnight in a standard fixative
200 solution (2.5% glutaraldehyde, 0.1 mol phosphate buffer, 1% sucrose, and pH 7.3) in
201 a refrigerator, and washed three to four times with phosphate buffered saline (PBS).
202 Samples were then post-fixed with 2% buffered $OsO_4$ for 2 h at room temperature,

203 and washed again with a buffer solution. Then, samples were dehydrated in a rising
204 propanol series (30%, 50%, 70% and 90%) for 3 min each and put in a 20 mg/ml
205 uranyl acetate solution for 25 min at 37°C to improve TEM contrast. Samples were
206 then embedded in propylene oxide with a rising amount of Epon resin (2:1, 1:1, 1:2)
207 for 60 min, and then with pure Epon resin overnight at room temperature. Semi-thin,
208 transverse sections with a ca. 500 nm thickness were cut with an ultra-microtome
209 (Leica Ultracut UCT, Leica Microsystems GmbH, Wetzlar, Germany). The semi-thin
210 sections were dyed with 0.5% toluidine blue and mounted for observation under a LM
211 (Zeiss Axio Lab.A1, Carl Zeiss Microscopy GmbH, Jena, Germany). Ultra-thin
212 sections with a 60-90 nm thickness were prepared with a diamond knife and put on
213 300 mesh copper grids or slotted grids.
214 Intervessel pit membranes were observed under a JEOL JEM-1400 TEM (Jeol
215 Germany GmbH, Freising, Germany), and TEM pictures were taken with a digital
216 camera (Soft Imaging System, Münster, Germany). Intervessel pit membrane
217 thickness ($T_{PM}$, nm) was measured based on TEM pictures using ImageJ (version
218 1.50i, National Institutes of Health, Bethesda, MD, USA). $T_{PM}$ was calculated as the
219 mean value of three measurements at opposite sides near the pit membrane annulus
220 and at the centre of the pit membrane. This approach was appropriate since pit
221 membranes in TEM images showed a largely homogeneous thickness across the entire
222 membrane. At least 15 different intervessel pits were measured for each sample.
223 Shrinkage of pit membranes for each species was calculated as:
224 $$\text{Shrinkage} = 100 * (T_{PM}\_F - T_{PM}\_DR) / T_{PM}\_F \,, \qquad \text{(Eqn 2)}$$

225 where $T_{PM}$_F and $T_{PM}$_DR represented the thickness of fresh and dried-rehydrated pit
226 membranes, respectively.

227 *The shrinkage model*

228 The shrinkage model developed included the following assumptions: (1) the thickness
229 of fresh pit membranes as seen under TEM is similar to the natural condition in plants,
230 (2) microfibril aggregates have a constant diameter of 20 nm, show a parallel
231 orientation to each other within a single layer, and a 45° shift in their orientation to
232 neighbouring layers, (3) there is an equal distance between cellulose layers within a
233 hydrated pit membrane, and (4) completely dried samples show fully shrunken pit
234 membranes, with a zero distance between each layer, and a zero distance between two
235 or three randomly grouped microfibril aggregates within a layer. A 3D visualisation of
236 a pit membrane with these assumptions is shown in Figure S1.

237 How realistic are these assumptions? It is currently unclear whether or not TEM
238 preparation is associated with any shrinkage of pit membranes. Microfibril aggregates
239 in pit membranes show a variable diameter, with values between 20 and 50 nm based
240 on SEM (Jansen et al., 2009). However, an average of 20 nm in fresh pit membranes
241 is considered to be realistic because SEM of dried samples is most likely
242 overestimating sizes due to an increase of the cellulose aggregate diameter between
243 wet and dried samples, additional aggregation of pre-aligned microfibrils, and/or due
244 to coating of proteins or unknown substances (Thimm et al., 2000). The assumption
245 that microfibril aggregates run in a parallel orientation, with a 45° orientation between
246 each layer is unrealistic. Yet, a completely random orientation of microfibril

247 aggregates is not compatible with a pit membrane model that is composed of layers of
248 microfibril aggregates, because a random orientation would imply a high amount of
249 overlap by overlaying microfibril aggregates. Despite the unrealistic nature of most
250 assumptions, an important question is whether or not these conditions show a major
251 effect on the 3D characteristics estimated. A more detailed discussion about this topic
252 is provided in the discussion.

253 Based on the 20 nm diameter of a single cellulose microfibril aggregate (d, nm), the
254 number of microfibril layers (N), was calculated as:

255 $N = T_{PM}\_DR / d$ , (Eqn 3)

256 where $T_{PM}\_DR$ was the mean thickness of dried pit membranes. The mean distance
257 between neighbouring cellulose microfibril aggregates (D, nm) could then be
258 estimated as:

259 $D = (T_{PM}\_F - T_{PM}\_DR) / (N - 1)$ , (Eqn 4)

260 where $T_{PM}\_F$ was the thickness of fresh pit membranes.

261 For a pit membrane with known values of N and D, the porosity (ε), geodesic
262 tortuosity (τ), and constrictivity (β) were calculated with the software GeoStoch
263 (Mayer, Schmidt, & Schweiggert, 2004).

264 *Colloidal gold perfusion experiments*

265 Colloidal gold perfusion experiments were applied to petioles and/or stems of seven
266 species, largely following Zhang et al. (2017). Colloidal gold particles suspended in a
267 0.1 mM PBS solution (100 µl $l^{-1}$ as $HAuCl_4$, pH6, Sigma-Aldrich, St. Louis, USA)
268 were used because they can easily be detected under TEM due to their high electron

density when $OsO_4$ is omitted as post-fixative. Also, gold particles with a wide range of diameters and precise, circular dimensions are available from various companies, while the red colour of the colloidal gold solution provides a relatively easy visual detection to see if the solution has fully perfused a sample. The disadvantage, however, is that colloidal gold particles are rather hydrophobic and slightly charged (Zhao, Li, & Astruc, 2013), which may determine interactions of gold particles with xylem sap compounds and inner vessel walls (see discussion).

Terminal branches were cut in the morning and kept in water. Then, adult petioles were re-cut under water to a length of 10 cm for *A. pseudoplatanus*, 3 cm for *C. camphora*, and 4 cm for *P. americana*. These lengths were close to the maximum petiole length of these species, and longer than the maximum vessel lengths measured in petioles of *A. pseudoplatanus* and *C. camphora*, which were 7.0 ± 1.3 cm and 2.3 ± 0.2 cm, respectively. The maximum vessel length for leaf samples (including the petiole and basal midrib) in *P. americana* was 6.4 ± 0.3 cm, which was longer than the 4 cm long petioles of this species. Maximum and mean vessel length data were based on silicon injection (Scholz et al., 2013). Fresh stem segments with a length that was 1.5 times the maximum stem vessel length (based on silicon injection, Scholz et al., 2013) were chosen for gold perfusion experiments. For the fresh samples, petioles and/or stems from seven species were submerged in distilled water and put under vacuum overnight to remove embolised conduits in xylem (Espino and Schenk, 2010). Comparison of directly embedded xylem tissue with xylem samples put under vacuum showed that the overnight vacuum condition had no effect on pit membrane

291 thickness.

292 To obtain dried-rehydrated samples, petioles from three species (*A. pseudoplatanus*, *C.*
293 *camphora*, and *P. americana*) were dried at room temperature until a minimum of
294 90% water loss was reached, which took at least 5 days. Relative water content was
295 determined by measuring the weight of the fresh and dried samples. Gradual drying of
296 xylem samples in earlier experiments showed that pit membranes were severely
297 shrunken when the xylem tissue showed 90% loss of water content (Kotowska et al.,
298 in press). The rehydration step under vacuum for 24 h facilitated not only injection of
299 colloidal gold, but also resin embedding during TEM preparation, athough TEM
300 preparation requires treatment with various chemicals that would also rehydrate dried
301 pit membranes.

302 Both fresh and dried-rehydrated samples were connected to a 60 cm column of
303 distilled water via a three-way stopcock, with an acropetal direction of water flow.
304 Samples were flushed with distilled water for 2-3 min. Although it is unclear whether
305 or not pore size dimensions change due to an ionic effect (Lee et al., 2012), the actual
306 injection was done with the 0.1 mM PBS solution of colloidal gold. Moreover, similar
307 experiments in which stem samples of various angiosperm species were flushed with
308 a 10 mM KCl solution or distilled water prior to gold perfusion, did not show a major
309 difference in the perfusion capacity of gold particles (Choat et al., 2003, 2004; Zhang
310 et al., 2017; Table 1). We prepared 1 ml of a 1:1:1:1 mixture of colloidal gold
311 solutions, with gold particles that had an average diameter of 5 nm (± 2 nm, lot
312 number MKCD4752), 10 nm (± 2 nm, lot number MKCC2817), 20 nm (± 2 nm, lot

313 number MKBZ7332V), and 50 nm (± 3 nm, lot number MKCB4933). This mixture
314 was injected in the system via a three-way stopcock. Although each colloidal gold
315 solution had a similar amount of gold per volume (100 μl $l^{-1}$ as $HAuCl_4$), solutions
316 with 5 and 10 nm gold particles contained much more gold particles for a given
317 volume than the 20 and 50 nm particle solutions. Gold particles of 5, 10, and 20 nm
318 provided information about the pit membrane pore size, while 50 nm particles were
319 assumed not to pass pit membranes (Choat et al., 2003; Choat et al., 2004; Zhang et
320 al., 2017). Therefore, the combination of smaller (5, 10 and 20 nm) colloidal gold
321 sizes with 50 nm particles was useful to determine conduits that were cut open at the
322 injection point. The perfusion was stopped when the red colour of the colloidal gold
323 solution was shown at the terminal end of the petiole, which took ca. 2-5 min under 6
324 kPa for fresh petioles of *A. pseudoplatanus* and *P. americana*, but about 30 min for *C.*
325 *camphora*.
326 The perfusion of dried-rehydrated petioles under 6 kPa took 20 min for *A.*
327 *pseudoplatanus*, but 45 min for *P. americana*, and several hours for *C. camphora*. The
328 slow flow rates for *C. camphora* and *P. americana* were most likely due to the small
329 conduit dimensions in their petioles and their relatively thick (> 500 nm) mean pit
330 membrane thickness. Therefore, we injected colloidal gold into both fresh and
331 dried-rehydrated petioles of the latter two species (*C. camphora* and *P. americana*) by
332 applying a 200 kPa pressure with a Scholander pressure chamber (Model 1000
333 Pressure Chamber Instrument, PMS Instrument Company, Albany OR, USA), which
334 took less than a minute. This pressure of 200 kPa was unlikely to cause mechanical

335 deformation and compression of pit membranes (Tixier et al., 2014). The increased
336 injection pressure of 200 kPa was not applied to petioles of *A. pseudoplatanus* since a
337 mean flow rate of 0.083 ± 0.014 mg $s^{-1}$ at 6 kPa was sufficient for this species.

338 *Colloidal gold detection*

339 The distribution and occurrence of gold particles in samples was examined under light
340 microscopy (LM) and TEM. For LM observations, transverse sections of 10-20 µm
341 thick from three to six petioles were made with a microtome (Schenkung Dapples,
342 Zürich, Switzerland) at the distal end of the injection point for *A. pseudoplatanus*, *C.*
343 *camphora*, and *P. americana*, which were at 9.5, 2.5, and 3.5 cm, respectively.
344 Sections were first treated for 8 min with 1 ml of a freshly made 1:1 mixture of
345 solution A and B from a silver enhancer kit (Sigma-Aldrich, St. Louis, USA). After
346 washing in distilled water, sections were fixated in 2.5% sodium thiosulfate for 2 min,
347 washed again in distilled water, and run through a graded alcohol series (50%, 60%,
348 70% and 100%) for 3 min. Finally, sections were transferred to a slide and embedded
349 in NeoMount (Merck KGaA, Darmstadt, Germany). Observations were made with a
350 LM (Zeiss Axio Lab.A1, Carl Zeiss Microscopy GmbH, Jena, Germany). Gold filled
351 vessels could easily be distinguished from non-filled vessels based on a dark staining
352 of the gold. The total number of vessels and the number of gold filled vessels were
353 counted in transverse sections using ImageJ. Then, the percentage of gold filled
354 vessels was calculated.

355 Gold particles in pit membranes could be observed under TEM with much greater
356 detail than LM. Several 1 x 2 x 2 mm xylem cubes from the middle of the samples

357 were cut under tap water for TEM preparation. Sample preparation for TEM was
358 performed as described above, but without applying $OsO_4$ treatment. Since no $OsO_4$
359 was used as post-fixative, pit membranes were highly transparent (Schenk et al., 2018;
360 Schenk et al., 2017; Jansen et al., 2018), and individual gold particles of all sizes
361 could easily be observed as circular, electron dense structures. $OsO_4$ treatment,
362 however, results in binding of Os to unsaturated fatty acid chains of lipids
363 (Riemersma, 1968), which results in dark, electron dense particles associated with pit
364 membranes. Therefore, Os-bound lipids could be mistaken for gold particles and
365 makes their visualisation more challenging.
366 Gold particles that were observed at a minimum distance of 50 nm from the pit
367 membrane surface were considered to be able to penetrate the pit membrane. This
368 criterion was easier and more reliable to determine the penetration capacity of
369 colloidal gold in intact pit membranes than determining whether or not a particular
370 conduit had an open end at the injection point. Open conduits could indeed be
371 observed based on the presence of 50 nm particles, but the relatively low amount of
372 50 nm particles compared to smaller gold sizes made it difficult to distinguish
373 non-open vessels from open vessels in a single transverse section. Since the presence
374 of 50 nm gold particles could be overlooked, the absence of 50 nm gold particles did
375 not provide solid evidence that a particular conduit represented a closed vessel.
376 *Statistics*
377 Statistical analyses were conducted in SPSS Statistics (Version 21, IBM Corporation,
378 Armonk, USA). A Shapiro-Wilk-Test was applied to test for the normal distribution of

379 data. An independent-samples t-test was applied with normally distributed data to
380 compare the means. If data were not normally distributed, the Mann-Whitney-U-Test
381 was used.
382 SigmaPlot 12.5 (Systat Software Inc., Erkrath, Germany) was used to prepare graphs
383 (Figure 3, Figure S2, S3), and 123D Design (Autodesk, Inc., San Rafael, USA) was
384 used to prepare a 3D image of a pit membrane (Figure. S1)
385

386 **Results**

387 *Pit membrane thickness measurements based on TEM*

388 Almost all intervessel pit membranes in fresh xylem samples showed a granular,
389 rather transparent appearance (Figure 2a, c, e). The granular structure of these pit
390 membranes was heterogeneous, resulting in a variable electron density across a single
391 pit membrane. Shrunken pit membranes, however, were also found in fresh stem
392 samples that had not been subject to any drying during preparation (Figure 2b, d, f).
393 The shrunken pit membranes were much thinner, darker and more electron dense than
394 the non-shrunken pit membranes. Moreover, shrunken pit membranes were generally
395 aspirated (Figure 2b, f) and show a homogeneous electron appearance with a dark line
396 at the outermost layer (Figure 2b, d).
397 The thickness of fresh pit membranes ($T_{PM}$_F) showed considerable variation (Table 2;
398 Figure 3), ranging from 172 ± 6 nm (mean ± SE) in *A. glutinosa* to 686 ± 18 nm in *C.*
399 *camphora*. Species from Mediterranean and tropical environments (including *C.*
400 *camphora*, *H. schizopetalus*, *N. oleander*, *P. americana*) showed thicker pit

401 membranes than those growing at the cool temperate climate in Ulm (*A. glutinosa*, *A.*
402 *pseudoplatanus*, *C. avellana*, *F. sylvatica*, *L. tulipifera*, *P. tremula*).
403 Dried-rehydrated pit membranes showed a thickness ($T_{PM}$_DR) ranging from 117 ± 3
404 nm in *F. sylvatica* to 370 ± 22 nm in *C. camphora* (Table 2). A significant difference
405 in thickness ($p < 0.05$) was found between fresh and dried-rehydrated pit membranes
406 for each species (Table 2). Shrunken pit membranes showed on average a 50.4 ± 2%
407 reduction of their thickness compared to fresh pit membranes (Figure 3). The largest
408 shrinkage of pit membranes was found for *C. avellana* (58.8%), and the lowest pit
409 membrane shrinkage was observed in *L. tulipifera* (41.7%). Both thin and thick pit
410 membranes appeared to show a similar shrinkage (Table 2; Figure 3). Moreover, fresh
411 pit membranes were found to be significantly thicker ($p < 0.001$) in petioles than in
412 stems for *A. pseudoplatanus*, *C. camphora*, and *P. americana* (Table 2).
413 *Estimation of porous medium characteristics based on a shrinkage model*
414 Pit membranes in petioles of *C. camphora* were composed of 18 layers of cellulose
415 aggregates, while 6 layers would occur in stems of *C. avellana* and *F. sylvatica* (Eqn 3;
416 Table 3). The estimated distance (D; Eqn 4) between cellulose layers ranged from
417 16.7 nm in stems of *L. tulipifera* to 33.5 nm in stems of *C. avellana* (Table 3). Overall,
418 the average distance between neighbouring layers of cellulose aggregates was 23.7 ±
419 2.1 nm for the seven species studied.
420 Moreover, fresh pit membranes showed a mean porosity of 0.81 ± 0.007 (Table 3),
421 while shrunken pit membranes had a mean porosity of 0.62 ± 0.001, which was
422 significantly different ($t(12) = 25.074$, $p < 0.001$) for seven species. Since the distance

423 between the cellulose layers was set to zero in dried pit membranes, the estimated
424 porosity of dried pit membranes was similar for all species. The geodesic tortuosity of
425 shrunken pit membranes (1.14 ± 0.005) was only slightly higher than the value of
426 fresh pit membranes (1.03 ± 0.001), although this difference was significant ($t(12) =$
427 $-22.230$, $p < 0.001$). Moreover, the constrictivity of fresh pit membranes (on average
428 0.76 ± 0.03) was higher than that of shrunken pit membranes (on average 0.66 ± 0.02,
429 n = 7 species), and this difference in constrictivity was also significant ($U = 6$, $p =$
430 $0.017$). An exception, however, was found for *C. avellana* (Table 3), which had a pit
431 membrane that was composed of only 6 cellulose layers and had the highest
432 inter-layer distance in our dataset (i.e., 33.5 nm for fresh pit membranes). The $R_{min}$
433 values (Eq. 1; Figure 1) of *C. avellana* calculated did not change for an inter-layer
434 distance above 27 nm. Therefore, the constrictivity values were lower for a fully
435 hydrated, fresh pit membrane of this species than a dried pit membrane.

436 *Gold perfusion based on LM*

437 Vessels with gold particles were visible as black stained walls in transverse sections at
438 the distal end of the injection point of petioles (Figure 4). There were few gold-filled
439 vessels after perfusion at 6 kPa in *A. pseudoplatanus*, but more in *P. americana*
440 (Figure S2). Injection of colloidal gold particles at 200 kPa significantly ($p < 0.05$)
441 increased the number of gold-filled vessels in *C. camphora* and *P. americana* (Figure
442 S2). Fresh and dried-rehydrated petioles showed no significant difference ($p > 0.05$)
443 in the percentage of gold-filled vessels for the three species studied, although the
444 mean values were considerably lower for dried-rehydrated samples of *C. camphora*

445 and *P. americana* (Figure S2).

446 The number of gold-filled vessels at the distal end in petioles of *C. camphora* and *P.*
447 *americana* was higher than the number of silicon filled vessels, with both colloidal
448 gold and silicon injected at a 200 kPa pressure (Figure S3). At a distance of 9.5 cm
449 from the injection point, the number of gold filled vessels in petioles of *A.*
450 *pseudoplatanus* after injection at 6 kPa was similar to the number of silicon filled
451 vessels injected at 200 kPa (Figure S2).

452 *Gold perfusion based on TEM*

453 Gold particles could be observed at the surface of pit membranes, on the pit border
454 walls, or on inner conduit walls in TEM pictures. Some grouping of colloidal gold
455 particles could be found, especially at places where electron dense substances were
456 found (Figure 5c, d; Figure 6a; Figure 7a, c), and some irregularly shaped, grey
457 particles clustering or coating the 20 and 50 nm gold particles can be seen (e.g. Figure
458 5c). Similar to the $OsO_4$ staining of pit membranes, this coating provides evidence for
459 the presence of lipids associated with colloidal gold. Moreover, the penetration of
460 gold particles was not homogeneously distributed across pit membranes. Gold
461 particles penetrating some parts of a pit membrane more easily than other areas were
462 frequently observed (Figure 5c; Figure 6a, c; Figure 7a, b), suggesting that pore sizes
463 were variable in size within a single pit membrane.

464 A summary of the pore sizes in pit membranes of seven species is given in Table 2.
465 Here, pore sizes in pit membranes were determined by the size of the smallest
466 colloidal gold particles that did not penetrate the pit membranes. In stems of *A.*

467 *glutinosa* and *A. pseudoplatanus*, 20 nm gold particles were found inside the fresh pit
468 membranes, but 50 nm gold particles remained on the outermost layers of fresh pit
469 membranes, which indicated a pore size < 50 nm for both species. Gold particles of
470 20 nm could not cross the fresh pit membranes in stems of *C. camphora*, *H.*
471 *schizopetalus*, *N. oleander*, and *P. americana* (Figure 7a) at 6 kPa, indicating a pore
472 size < 20 nm in these four species.

473 Pore sizes < 50 nm (Table 2; Figure 5a, c) were found for fresh petioles and stems of
474 *A. pseudoplatanus*. For fresh petioles of *C. camphora* perfused at 200 kPa (Figure 6a,
475 c), the pore size was < 20 nm, which was similar to the size found in stems perfused
476 at 6 kPa (Table 2). At 6 kPa, however, 5 and 10 nm gold particles were not observed
477 within pit membranes from fresh petioles of this species. Moreover, 20 nm gold
478 particles could not enter pit membranes in fresh petioles of *P. americana* perfused
479 both at 6 and 200 kPa, showing a pore size < 20 nm for fresh petioles (Figure 7b) and
480 stems (Figure 7a).

481 For dried-rehydrated petioles of *A. pseudoplatanus*, *C. camphora*, and *P. americana*,
482 the estimated pore sizes were consistently smaller than in fresh samples. No 20 nm
483 gold particles penetrated dried-rehydrated pit membranes in *A. pseudoplatanus* at 6
484 kPa (Table 2; Figure 5b, d). Dried-rehydrated pit membranes in petioles of *C.*
485 *camphora* and *P. americana* suggested a pore size < 5 nm both at 6 and 200 kPa
486 (Table 2; Figure 6b, d; Figure 7c).

487

488 **Discussion**

One of the most interesting findings is that our results show good agreement in pore sizes of pit membranes between the two independent approaches followed, namely the shrinkage model and gold perfusion experiments. Pore size diameters in intact, hydrated pit membranes are well below 50 nm, and typically below 20 nm. These values are in general agreement with earlier gold perfusion experiments (Choat et al., 2003, 2004; Zhang et al., 2017), and suggest that much larger pores (> 100 nm) based on SEM are likely preparation artefacts that do not occur in intact, hydrated pit membranes of angiosperms (Hillabrand et al., 2016; Jansen et al., 2009; Sano, 2005). Two additional, novel findings concern estimations of porous medium characteristics, and preliminary evidence that pore sizes might be related to pit membrane thickness. Finally, drying of pit membranes was found to result in reduced pore sizes. These findings raise various questions with respect to water transport across intervessel pits, and especially air-seeding, but should also be discussed critically with respect to shortcomings and limitations of the modelling and experimental methods applied.

***A critical evaluation of pore size dimensions based on modelling and gold perfusion***

Despite the striking agreement between the shrinkage model and gold perfusion results, some caution is required for the interpretation of our pore size dimensions. An important assumption made in our shrinkage model is the hypothesis that TEM images of freshly embedded pit membranes represent the actual pit membrane thickness of intact, hydrated pit membranes in the plant. Importantly, observation of intervessel pit membranes with confocal laser scanning microscopy, which requires no dehydration or any chemical treatment, showed pillow-shaped structures with a

511 much thicker appearance than TEM images of freshly embedded material (Schenk et
512 al., 2018). Therefore, it is possible that sample dehydration by alcohol during TEM
513 preparation may cause some artificial shrinkage. Such shrinkage is likely because pit
514 membranes represent apoplastic structures not protected by a cell membrane. While
515 this requires further research, a potential shrinkage artefact by TEM preparation is
516 likely to affect all samples equally as long as the sample preparation and treatment are
517 similar, which means that TEM would provide relative pit membrane thickness data.
518 While gold concentrations in the perfusate were typically too low for quantification
519 based on microwave plasma atomic emission spectrometry (data not shown), light
520 microscopy provided clear visualisation of vessels with or without gold, but did not
521 enable us to distinguish vessels that were cut-open at the injection side from non-open
522 vessels. Therefore, TEM provided a more accurate and direct visualisation of the
523 permeability of intervessel pit membranes than analytical detection or light
524 microscopy. When we omitted $OsO_4$, TEM observation allowed us to distinguish
525 small (5 and 10 nm) gold particles inside pit membranes. Similar to many previous
526 TEM observations (e.g., Schmid and Machado, 1968; Jansen et al., 2009; Schenk et
527 al., 2017), the application of $OsO_4$ provided evidence for the occurrence of lipids on
528 inner walls of conduits, including pit borders and pit membranes, and also indicated
529 that lipids cluster around gold particles (e.g., Figure 5c). The coating of gold particles
530 by amphiphilic lipids could affect the size and penetration capacity of pit membranes
531 pores. Besides the hydrophobic and charged nature of the colloidal gold particles,
532 their perfusion may also be affected by electroviscosity (Santiago, Pagay, & Stroock,

533 2013) and impenetrable boundary layers (Sulbaran, Toriz, Allan, Pollack, & Delgado,
534 2014). Therefore, our TEM observations of gold perfused xylem may represent a
535 relative indication of pore sizes, and it is possible that pore constrictions are slightly
536 larger than what we experimentally measured. Yet, lipid coating, electric charging,
537 and boundary layer effects may result in nanoscale artefacts, and do not explain the
538 much larger pore sizes (> 100 nm) observed with SEM.
539 Assuming a random arrangement of microfibril aggregates, constriction sizes in pores
540 have a normal distribution. Therefore, it is unclear why some areas of the pit
541 membrane were found to have smaller constriction sizes than other areas, although
542 local changes in the clustering of microfibril aggregates could provide an explanation.
543 Moreover, thick pit membranes appear to show smaller pore sizes than thin pit
544 membranes, with pore constrictions < 20 nm for four species with thick (> 300 nm)
545 pit membranes, and pore constrictions < 50 nm for three species with a thin (< 300 nm)
546 pit membrane. It is obvious that thick pit membranes with a long pore will have more
547 constrictions than a thin pit membrane with a short pore. Therefore, the probability is
548 higher that a long pore includes a really small constriction than a short pore. This is
549 especially relevant because gold particle penetration and air-seeding is determined by
550 the minimum constriction and not by the average or largest constriction within a pore.
551 Since the relationship between pit membrane thickness and pore size was supported
552 by our gold perfusion data only, and not by our shrinkage model, this observation
553 requires testing on a larger number of species.
554 ***Pore sizes in dried, shrunken pit membranes become generally reduced***

555 Contrary to what we expected, pit membrane shrinkage by drying did not cause large
556 pores in intervessel pit membranes as reported for *Drimys winteri* (Zhang et al., 2017).
557 Instead, our gold perfusion experiments show considerably small pores sizes in dried
558 pit membranes of *A. pseudoplatanus*, *C. camphora*, and *P. americana*. This apparent
559 contradiction could be explained by differences in pit membrane thickness and
560 re-arrangement of microfibril aggregates during dehydration. Thick pit membranes in
561 fresh material are likely to have many microfibril layers, which are more likely to
562 form a fairly closed, dense network when shrunken compared to thin pit membranes
563 with a few layers only. Thus, relatively thick pit membranes may not show large pores
564 when many layers of microfibril aggregates become tightly compressed after
565 dehydration. On the other hand, rearrangement of microfibril aggregates during
566 dehydration is likely to create few large openings if the pit membrane consists of few
567 layers only. In fact, large pores in dried pit membranes have especially been observed
568 with SEM in species with thin pit membranes, such as *Populus tremuloides*, *P.*
569 *balsaminifera*, *Salix alba*, *Aesculus hippocastanum*, and some vesselless angiosperms
570 (Table 1; Hillabrand et al., 2016; Jansen et al., 2009; Sperry, Perry, & Sullivan, 1991;
571 Zhang et al., 2017). The effect of pit membrane thickness of pore sizes in SEM is also
572 clear when a few microfibril layers have been peeled off during sample preparation
573 (e.g., Figure 2c in Jansen et al., 2009). Nevertheless, pit membranes in *A.*
574 *pseudoplatanus* are only slightly thicker under TEM than those of *Drimys winteri*
575 (Zhang et al., 2017), suggesting that differences in pit membrane chemistry (e.g.,
576 proteins, lipids, or lipoproteins) might also affect the spatial arrangement of

577 microfibril aggregates within pit membranes.

578 The most likely reason why aggregation of cellulose fibrils and pit membrane
579 shrinkage is irreversible, is the formation of hydrogen bonds between glucose chains
580 of cellulose molecules after removal of water molecules from the hydration shell that
581 normally separates cellulose molecules from each other (Fang & Catchmark, 2014;
582 Martínez-Sanz, Pettolino, Flanagan, Gidley, & Gilbert, 2017). This process is similar
583 to fibre hornification, which describes structural changes of cellulose fibres in wood
584 pulp or paper during oven drying or water removal by the formation of largely
585 irreversible hydrogen bonding (Chen et al., 2018; Diniz, Gil, & Castro 2004).

586 ***The functional significance of pit membrane porosity, geodesic tortuosity, and***
587 ***constrictivity***

588 Since high porosity values between 80% and 95% are characteristic of non-woven
589 porous media composed of fibrils (Shou, Fan, & Ding, 2011; Vallabh, Banks-Lee,
590 Seyam, 2010; Vallabh, Ducoste, Seyam, & Banks-Lee, 2011), it is not surprising that
591 pit membranes possess a considerably high porosity, with a mean porosity of 81% for
592 fresh pit membranes based on our shrinkage model. This means that the solid material
593 of a pit membrane represents typically less than 20% of the pit membrane volume,
594 with a relatively thin and only sporadically touching 3D network of microfibril
595 aggregates. Because shrinkage of pit membranes results in a more compact
596 arrangement of cellulose with typically reduced pore volumes, a mean porosity of
597 62% for dried pit membranes seems reasonable, and it can be expected that actual
598 pore tissue fractions of fresh and dried pit membranes show even larger differences.

Also, the reduced porosity of dried pit membranes does not exclude the likelihood that a few large pores can be created in a relatively thin pit membrane.

The low geodesic tortuosity values are not uncommon for fibrous porous media (Huang et al., 2015; Bini, Pica, Marinozzi, & Marinozzi, 2019; Holzer et al., 2013; Stenzel, Pecho, Holzer, Neumann, & Schmidt, 2016), and indicate that pit membranes do not consist of a highly tortuous, bent, or zigzagging pathway, despite its geometrically highly irregular pore shapes and volumes. Therefore, pit membranes provide hydraulic pathways that are close to the shortest pathway, without considerably extending the hydraulic pathway of xylem sap.

The relatively high values of constrictivity values for fresh pit membranes suggest that these can be compared to a stack of sieves, with plenty of space between and within the sieves, and mainly non-touching aggregates of microfibril aggregates. While many porous structures exhibit lower constrictivity values, the estimated values are not uncommon (Holzer et al., 2013; Stenzel et al., 2016; Westhoff et al., 2018), and suggest that pore constrictions (also called pore throats) occur. Constrictions are functionally important for air-seeding of pit membranes, which requires also more attention by insoluble, amphiphilic lipids with a concentration dependent surface tension in xylem sap and conduits (Scott, Sjaholm, & Bowler, 1960; Esau, Cheadle, & Gill, 1966; Schenk et al., 2017, 2018). Since the pore pathway followed by an air-water meniscus includes large pore volume changes, with at least a few pore constrictions, bubble snap-off events (or Haines jumps) may occur when a constriction has ≤ ½ the diameter of the pore volume on either side of the constriction

621 (Gido, Hirt, Montgomery, Prud'homme, & Rebenfeld, 1989; Schenk et al., 2015).
622 Therefore, the concept of pit membrane constrictivity has considerable implications
623 for air-seeding, with the smallest constriction in a pore representing the main
624 hydraulic bottleneck.

625 ***The functional significance of pore sizes for air-seeding***

626 How likely is air-seeding through a 20 nm pore size, which is close to the pore size
627 estimations based on our shrinkage model and gold perfusion experiments? According
628 to the Young Laplace equation, the pressure difference forcing a bubble through a 20
629 nm pore, assuming a contact angle of zero (Caupin, Cole, Balibar, & Treiner, 2008;
630 Meyra et al., 2007), and a pore shape correction factor of 0.5 (Schenk et al., 2015),
631 would be 7.2 MPa in pure water. Because surface-active substances, such as
632 phospholipids, are known to occur in xylem sap and to be associated with pits (Jansen
633 et al., 2018; Schenk et al., 2018; Schenk et al., 2017), the surface tension inside pores
634 is likely to be much reduced. If the surface tension of an air-water meniscus is
635 reduced to 24 mJ $m^{-2}$, which is a typical equilibrium surface tension for phospholipid
636 monolayers (Lee, Kim, & Needham, 2001), a meniscus could pass through a 20 nm
637 pore with a shape correction factor of 0.5 under a pressure difference of 2.4 MPa.
638 Conversely, air-seeding pressures of 1 and 2 MPa would correspond to pore sizes of
639 48 and 24 nm for a surface tension of 24 mJ $m^{-2}$, but pore sizes would be much higher
640 in pure water, with pores of 144 and 72 nm for 1 and 2 MPa air-seeding pressure,
641 respectively.

642 Although the actual surface tension of an air-water meniscus on/within pit membranes

is uncertain, the narrow pore sizes observed in earlier studies and in this paper raise questions about the classic air-seeding mechanism. Clearly, embolisms form in almost all plant species at pressure differences far less than the 7.2 MPa predicted for 20 nm pores if sap was pure water, and for most species also at pressure differences less than 2.4 MPa predicted for surface tension in the presence of surface-active lipids. So, if membrane pores are so small, how do these embolisms form? Moreover, drought-induced embolisms also develop in conduits that are not connected to any embolised conduit (Choat et al., 2016; Choat, Brodersen, & McElrone, 2015; Choat et al., 2012; Knipfer, Brodersen, Zedan, Kluepfel, & McElrone, 2015). A common explanation is that there are a few enlarged pores that will make any conduit vulnerable to air seeding (Plavcová, Jansen, Klepsch, & Hacke, 2013), but, enlarged pores are typically not observed in the relatively low number of pit membranes that can be studied with TEM (Christman, Sperry, & Adler, 2009; Christman, Sperry, & Smith, 2012; Wheeler, Sperry, Hacke, & Hoang, 2005) or atomic force microscopy (Pesacreta et al., 2005). Clearly, the artifactual pores observed under SEM should be discounted as evidence for rare, large pores (Jansen, Pletsers, & Sano, 2008).

Our finding of reduced pore sizes in dried, shrunken pit membranes suggests that pit membrane dehydration after embolism should make pit membranes less prone to air seeding, not more, as predicted based on air-seeding fatigue (i.e., cavitation fatigue), where embolism increases the chance of subsequent embolism formation (Hacke, Stiller, Sperry, Pittermann, & McCulloh, 2001) in *Aesculus hippocastanum*, *Helianthus annuus*, *Populus angustifolia*, and *P. tremuloides* (Hacke et al., 2001;

Stiller & Sperry, 2002; Hillabrand et al., 2016). The thin and flimsy pit membranes of *Aesculus hippocastanum* and *Populus* (Jansen et al., 2009) may be more prone to developing large pores after dehydration than species with thicker pit membranes, which might hold up capillary water for a longer time after embolism, although this requires further testing. Although our findings confirm that pit membrane shrinkage occurs not only under experimental drying in the lab, but also happens in plants in the field, it is currently unknown how fast pit membranes dehydrate after embolism formation in a plant, and whether or not potential shrinkage is also caused by mechanical stretching during pit membrane aspiration.

***Conclusion***

Both our modelling approach and gold perfusion experiments provide clear evidence for a maximum size of pit membrane pores well below 50 nm, while the porosity, geodesic tortuosity, and constrictivity values calculated are characteristic of non-woven, fibrous porous media. Dehydration of pit membranes leads to significant changes in these porous medium characteristics, such as a reduction of porosity. While enlarged pores may occur in thin pit membranes after drying, pore sizes become typically very small when pit membranes dehydrate. We also report preliminary evidence for a correlation between pore size and fresh pit membrane thickness. Further work is needed to obtain information about the pit membrane thickness in fully hydrated, fresh samples, as well as ultrastructural observations of cellulose microfibril aggregates in never-dried pit membranes, which would also be essential to develop a 3D pit membrane model based on actual images. The

development of such a pit membrane model and its porous medium characteristics will allow us to make progress in understanding flow through pit membranes, pit membrane permeability, the hydraulic resistance offered by a pit membrane, air-seeding, and the longstanding question of water transport under negative pressure.

**Acknowledgements**

We thank Andrea Huppenberger for technical assistance and Jutta Siegmund-Jonietz for providing plant material. We thank Anna Bazle, Dewen Qin, Manon Peuker, Nora Deuter, Rebecca Thom, Sandra Schiele, and Susanne Ailinger for TEM observations, and Sean Gleason and Clemens Altaner for providing useful comments on an earlier version of this paper. The Electron Microscopy Section of Ulm University is acknowledged for technical support with electron microscopy. Financial support was provided by the DFG (JA 2174/5-1; nr. 383393940), NSF (IOS-1754850), and the MWK Baden-Württemberg (Ideenwettbewerb Biotechnologie). Y.Z. acknowledges financial support from the Chinese Scholarship Council.

**Conflict of interest**

We declare that we have no conflict of interest.

**Author Contribution**

Z.Y., S.H.J., K.M., and J.S. designed the research; Z.Y., M.T., K.M., W.M., K.M.M., C.C., and K.L. performed the research; W.P. contributed microscopy; Z.Y., S.H.J.,

S.V., and J.S. wrote the manuscript, with the contribution from all authors.

## References

Bhattad, P., Willson, C. S., & Thompson, K. E. (2011). Effect of network structure on characterization and flow modeling using X-ray micro-tomography images of granular and fibrous porous media. *Transport in Porous Media*, *90*(2), 363–391.

Bini, F., Pica, A., Marinozzi, A., & Marinozzi, F. (2019). A 3D model of the effect of tortuosity and constrictivity on the diffusion in mineralized collagen fibril. *Scientific Reports*, *9*(1), 2658.

Brodersen, C., & McElrone, A. (2013). Maintenance of xylem network transport capacity: a review of embolism repair in vascular plants. *Frontiers in Plant Science*, *4*, 108.

Caupin, F., Cole, M. W., Balibar, S., & Treiner, J. (2008). Absolute limit for the capillary rise of a fluid. *EPL(Europhysics Letters)*, *82*(5), 56004.

Chen, Y., Jiang, Y., Wan, J., Wu, Q., Wei, Z., & Ma, Y. (2018). Effects of wet-pressing induced fiber hornification on hydrogen bonds of cellulose and on properties of eucalyptus paper sheets. *Holzforschung*, *72*(10), 829–837.

Choat, B., Badel, E., Burlett, R., Delzon, S., Cochard, H., & Jansen, S. (2016). Noninvasive measurement of vulnerability to drought-induced embolism by X-ray microtomography. *Plant Physiology*, *170*(1), 273–282.

Choat, B., Ball, M., Luly, J., & Holtum, J. (2003). Pit membrane porosity and water stress-induced cavitation in four co-existing dry rainforest tree species. *Plant Physiology*, *131*(1), 41–48.

Choat, B., Brodersen, C. R., & McElrone, A. J. (2015). Synchrotron X-ray microtomography of xylem embolism in *Sequoia sempervirens* saplings during cycles of drought and recovery. *New Phytologist*, *205*(3), 1095–1105.

Choat, B., Cobb, A. R., & Jansen, S. (2008). Structure and function of bordered pits: new discoveries and impacts on whole-plant hydraulic function. *New Phytologist*, *177*(3), 608–626.

Choat, B., Jansen, S., Brodribb, T. J., Cochard, H., Delzon, S., Bhaskar, R., ... Zanne, A. E. (2012). Global convergence in the vulnerability of forests to drought. *Nature*, *491*(7426), 752–755.

Choat, B., Jansen, S., Zwieniecki, M. A., Smets, E., & Holbrook, N. M. (2004). Changes in pit membrane porosity due to deflection and stretching: the role of vestured pits. *Journal of Experimental Botany*, *55*(402), 1569–1575.

Christman, M. A., Sperry, J. S., & Adler, F. R. (2009). Testing the 'rare pit' hypothesis for xylem cavitation resistance in three species of *Acer*. *New Phytologist*, *182*(3), 664–674.

Christman, M. A., Sperry, J. S., & Smith, D. D. (2012). Rare pits, large vessels and extreme vulnerability to cavitation in a ring-porous tree species. *New Phytologist*, *193*(3), 713–720.

Crombie, D. S., Hipkins, M. F., & Milburn, J. A. (1985). Gas penetration of pit membranes in the xylem of *Rhododendron* as the cause of acoustically detectable sap cavitation. *Functional Plant Biology*, *12*(5), 445–453.

Diniz, J. F., Gil, M. H., & Castro, J. A. A. M. (2004). Hornification—its origin and interpretation in wood pulps. *Wood Science and Technology*, *37*(6), 489–494.

Esau, K., Cheadle, V. I., & Gill, R. H. (1966). Cytology of differentiating tracheary elements II. Structures associated with cell surfaces. *American Journal of Botany*, *53*(8), 765–771.

Espino, S., & Schenk, H. J. (2010). Mind the bubbles: achieving stable measurements of maximum hydraulic conductivity through woody plant samples. *Journal of Experimental Botany*, *62*(3), 1119–1132.

Fang, L., & Catchmark, J. M. (2014). Structure characterization of native cellulose during dehydration and rehydration. *Cellulose*, *21*(6), 3951–3963.

Gido, S. P., Hirt, D. E., Montgomery, S. M., Prud'homme, R. K., & Rebenfeld, L. (1989). Foam bubble size measured using image analysis before and after passage through a porous medium. *Journal of Dispersion Science and Technology*, *10*(6), 785–793.

Gleason S. M., Westoby M., Jansen S., Choat B., Hacke U. G., Pratt R.B., ... Zanne A.E. (2015). Weak tradeoff between xylem safety and xylem-specific hydraulic efficiency across the world's woody plant species. *New Phytologist*, *209*(1), 123–136.

Hacke, U. G., Stiller, V., Sperry, J. S., Pittermann, J., & McCulloh, K. A. (2001). Cavitation fatigue. Embolism and refilling cycles can weaken the cavitation resistance of xylem. *Plant Physiology*, *125*(2), 779–786.

Harvey, H. P., & van den Driessche, R. (1997). Nutrition, xylem cavitation and drought resistance in hybrid poplar. *Tree Physiology*, *17*(10), 647–654.

Hillabrand, R. M., Hacke, U. G., & Lieffers, V. J. (2016). Drought-induced xylem pit membrane damage in aspen and balsam poplar. *Plant, Cell & Environment*, *39*(10), 2210–2220.

Holzer, L., Wiedenmann, D., Münch, B., Keller, L., Prestat, M., Gasser, P., Robertson. I., & Grobéty, B. (2013). The influence of constrictivity on the effective transport properties of porous layers in electrolysis and fuel cells. *Journal of Materials Science*, *48*(7), 2934–2952.

Huang, X., Wang, Q., Zhou, W., Deng, D., Zhao, Y., Wen, D., & Li, J. (2015). Morphology and transport properties of fibrous porous media. *Powder Technology*, *283*, 618–626.

Jane, F. W. (1956). *The Structure of Wood*. Adam & Charles Black, London.

Jansen, S., Choat, B., & Pletsers, A. (2009). Morphological variation of intervessel pit membranes and implications to xylem function in angiosperms. *American Journal of Botany*, *96*(2), 409–419.

Jansen, S., Klepsch, M., Li, S., Kotowska, M. M., Schiele, S., Zhang, Y., & Schenk, H. J. (2018). Challenges in understanding air-seeding in angiosperm xylem. *Acta Horticulturae*, *1222*, 13–20.

Jansen, S., Pletsers, A., & Sano, Y. (2008). The effect of preparation techniques on SEM-imaging of pit membranes. *IAWA Journal*, *29*(2), 161–178.

Jansen S., & Schenk H. J. (2015). On the ascent of sap in the presence of bubbles. *American Journal of Botany*, *102*(10), 1–3.

Jarbeau, J. A., Ewers, F. W., & Davis, S. D. (1995). The mechanism of water-stress-induced embolism in two species of chaparral shrubs. *Plant, Cell & Environment*, *18*(2), 189–196.

Klepsch M., Lange A., Angeles G., Mehltreter K., Jansen S. (2016) The hydraulic architecture of petioles and leaves in tropical fern species under different levels of canopy openness. *International Journal of Plant Sciences*, *177*(2): 209–216.

Knipfer, T., Brodersen, C. R., Zedan, A., Kluepfel, D. A., & McElrone, A. J. (2015). Patterns of drought-induced embolism formation and spread in living walnut saplings visualized using X-ray microtomography. *Tree Physiology*, *35*(7), 744–755.

Kovscek, A. R., & Radke, C. J. (1996). Gas bubble snap-off under pressure-driven flow in constricted noncircular capillaries. *Colloids and Surfaces A: Physicochemical and Engineering Aspects*, *117*(1-2), 55–76.

Lee, J., Holbrook, N. M., & Zwieniecki, M. A. (2012). Ion induced changes in the structure of bordered pit membranes. *Frontiers in Plant Science*, *3*, 55.

Lee, S., Kim, D. H., & Needham, D. (2001). Equilibrium and dynamic interfacial tension measurements at microscopic interfaces using a micropipet technique. 2.

Dynamics of phospholipid monolayer formation and equilibrium tensions at the water – air interface. *Langmuir*, *17*(18), 5544–5550.

Lens, F., Sperry, J. S., Christman, M. A., Choat, B., Rabaey, D., & Jansen, S. (2011). Testing hypotheses that link wood anatomy to cavitation resistance and hydraulic conductivity in the genus *Acer*. *New Phytologist*, *190*(3), 709–723.

Li, S., Lens, F., Espino, S., Karimi, Z., Klepsch, M., Schenk, H. J., ... & Jansen, S. (2016). Intervessel pit membrane thickness as a key determinant of embolism resistance in angiosperm xylem. *IAWA Journal*, *37*(2), 152–171.

Martínez-Sanz, M., Pettolino, F., Flanagan, B., Gidley, M. J., & Gilbert, E. P. (2017). Structure of cellulose microfibrils in mature cotton fibres. *Carbohydrate Polymers*, *175*, 450–463.

Mayer, J., Schmidt, V., & Schweiggert, F. (2004). A unified simulation framework for spatial stochastic models. *Simulation Modelling Practice and Theory*, *12*(5), 307–326.

McCully, M., Canny, M., Baker, A., & Miller, C. (2014). Some properties of the walls of metaxylem vessels of maize roots, including tests of the wettability of their lumenal wall surfaces. *Annals of Botany*, *113*(6), 977–989.

Meyra, A. G., Kuz, V. A., & Zarragoicoechea, G. J. (2007). Geometrical and physicochemical considerations of the pit membrane in relation to air seeding: the pit membrane as a capillary valve. *Tree Physiology*, *27*(10), 1401–1405.

Morris, H., Brodersen, C., Schwarze, F. W. M. R., & Jansen, S. (2016). The Parenchyma of secondary xylem and its critical role in tree defense against fungal decay in relation to the CODIT model. *Frontiers in Plant Science*, *7*, 1665.

Neumann, M., Stenzel, O., Willot, F., Holzer, L., & Schmidt, V. (2019). Quantifying the influence of microstructure on effective conductivity and permeability: virtual materials testing. *International Journal of Solids and Structures*, in press.

Plavcová L, Jansen S, Klepsch M, & Hacke UG. (2013). Nobody's perfect: can irregularities in pit structure influence vulnerability to cavitation? *Frontiers in Plant Science*, *4*, 453.

Pesacreta, T. C., Groom, L. H., & Rials, T. G. (2005). Atomic force microscopy of the intervessel pit membrane in the stem of *Sapium sebiferum* (Euphorbiaceae). *IAWA Journal*, *26*(4), 397–426.

Petersen, E. E. (1958). Diffusion in a pore of varying cross section. *AIChE Journal*, *4*(3), 343–345.

Riemersma, J. C. (1968). Osmium tetroxide fixation of lipids for electron microscopy a possible reaction mechanism. *Biochimica Et Biophysica Acta (BBA)-Lipids and Lipid Metabolism*, *152*(4), 718–727.

Roof, J. G. (1970). Snap-off of oil droplets in water-wet pores. *Society of Petroleum Engineers Journal*, *10*(01), 85–90.

Sano, Y. (2005). Inter-and intraspecific structural variations among intervascular pit membranes, as revealed by field-emission scanning electron microscopy. *American Journal of Botany*, *92*(7), 1077–1084.

Sano, Y, Morris, H., Shimada, H., Ronse De Craene, L. P., & Jansen, S. (2011). Anatomical features associated with water transport in imperforate tracheary elements of vessel-bearing angiosperms. *Annals of Botany*, *107*(6), 953–964.

Santiago, M., Pagay, V., & Stroock, A. D. (2013). Impact of electroviscosity on the hydraulic conductance of the bordered pit membrane: a theoretical investigation. *Plant Physiology*, *163*(2), 999–1011.

Schenk, H. J., Espino, S., Rich-Cavazos, S. M., & Jansen, S. (2018). From the sap's perspective: The nature of vessel surfaces in angiosperm xylem. *American Journal of Botany*, *105*(2), 172–185.

Schenk, H. J., Espino, S., Romo, D. M., Nima, N., Do, A. Y. T., Michaud, J. M., ... Jansen, S. (2017). Xylem surfactants introduce a new element to the cohesion-tension theory. *Plant Physiology*, *173*(2), 1177–1196.

Schenk, H. J., Steppe, K., & Jansen, S. (2015). Nanobubbles: a new paradigm for air-seeding in xylem. *Trends in Plant Science*, *20*(4), 199–205.

Schmid, R., & Machado, R. D. (1968). Pit membranes in hardwoods—fine structure and development. *Protoplasma*, *66*(1-2), 185–204.

Scholz, A., Rabaey, D., Stein, A., Cochard, H., Smets, E., & Jansen, S. (2013). The evolution and function of vessel and pit characters with respect to cavitation resistance across 10 *Prunus* species. *Tree Physiology*, *33*(7), 684–694.

Scott, F. M., Sjaholm, V., & Bowler, E. (1960). Light and electron microscope studies of the primary xylem of *Ricinus communis*. *American Journal of Botany*, *47*(3), 162–173.

Shane, M. W., McCully, M. E., & Canny, M. J. (2000). Architecture of branch-root junctions in maize: structure of the connecting xylem and the porosity of pit membranes. *Annals of Botany*, *85*(5), 613–624.

Shou, D., Fan, J., & Ding, F. (2011). Hydraulic permeability of fibrous porous media. *International Journal of Heat and Mass Transfer*, *54*(17-18), 4009–4018.

Sperry, J. S., Hacke, U. G., & Pittermann, J. (2006). Size and function in conifer tracheids and angiosperm vessels. *American Journal of Botany*, *93*(10), 1490–1500.

Sperry, J. S., Perry, A. H., & Sullivan, J. E. M. (1991). Pit membrane degradation and air-embolism formation in ageing xylem vessels of *Populus tremuloides* Michx. *Journal of Experimental Botany*, *42*(11), 1399–1406.

Sperry, J. S., & Tyree, M. T. (1988). Mechanism of water stress-induced xylem embolism. *Plant Physiology*, *88*(3), 581–587.

Stenzel, O., Pecho, O., Holzer, L., Neumann, M., & Schmidt, V. (2016). Predicting effective conductivities based on geometric microstructure characteristics. *AIChE Journal*, *62*(5), 1834–1843.

Stiller, V., & Sperry, J. S. (2002). Cavitation fatigue and its reversal in sunflower (*Helianthus annuus* L.). *Journal of Experimental Botany*, *53*(371), 1155–1161.

Sulbaran, B., Toriz, G., Allan, G. G., Pollack, G. H., & Delgado, E. (2014). The dynamic development of exclusion zones on cellulosic surfaces. *Cellulose*, *21*(3), 1143–1148.

Thimm, J. C., Burritt, D. J., Ducker, W. A., & Melton, L. D. (2000). Celery (*Apium graveolens* L.) parenchyma cell walls examined by atomic force microscopy: effect of dehydration on cellulose microfibrils. *Planta*, *212*(1), 25–32.

Tixier, A., Herbette, S., Jansen, S., Capron, M., Tordjeman, P., Cochard, H., & Badel, E. (2014). Modelling the mechanical behaviour of pit membranes in bordered pits with respect to cavitation resistance in angiosperms. *Annals of Botany*, *114*(2), 325–334.

Vallabh, R., Banks-Lee, P., & Seyam, A. F. (2010). New Approach for determining tortuosity in fibrous porous media. *Journal of Engineered Fabrics & Fibers (JEFF)*, *5*(3), 7–15.

Vallabh, R., Ducoste, J., Seyam, A. F., & Banks-Lee, P. (2011). Modeling tortuosity in thin fibrous porous media using computational fluid dynamics. *Journal of Porous Media*, *14*(9), 791–804.

van Brakel, J., & Heertjes, P. M. (1974). Analysis of diffusion in macroporous media in terms of a porosity, a tortuosity and a constrictivity factor. *International Journal of Heat and Mass Transfer*, *17*(9), 1093–1103.

Westhoff, D., Skibinski, J., Šedivý, O., Wysocki, B., Wejrzanowski, T., & Schmidt, V. (2018). Investigation of the relationship between morphology and permeability for open-cell foams using virtual materials testing. *Materials & Design*, *147*, 1–10.

Wheeler, J. K., Sperry, J. S., Hacke, U. G., & Hoang, N. (2005). Inter-vessel pitting and cavitation in woody Rosaceae and other vesselled plants: a basis for a safety

versus efficiency trade-off in xylem transport. *Plant, Cell & Environment*, *28*(6), 800–812.

Williamson, V., & Milburn, J. A. (2017). Xylem vessel length and distribution: does analysis method matter? A study using *Acacia*. *Australian Journal of Botany*, *65*(3), 292–303.

Zhang, Y., Klepsch, M., & Jansen, S. (2017). Bordered pits in xylem of vesselless angiosperms and their possible misinterpretation as perforation plates. *Plant, Cell & Environment*, *40*(10), 2133–2146.

Zhao, P., Li, N., & Astruc, D. (2013). State of the art in gold nanoparticle synthesis. *Coordination Chemistry Reviews*, *257*(3-4), 638–665.

Zimmermann, M. H. (1983). *Xylem Structure and the Ascent of Sap*. Springer Science & Business Media.

Zimmermann, M. H., & Brown, C. L. (1971). *Trees: Structure and Function*. New York, USA, Springer-Verlag..

## Supporting Information

Additional Supporting Information may be found online in the supporting information tab for this article.

**Figure S1.** A three-dimensional (3D) intervessel pit membrane model of angiosperms showing the effect of dehydration on a pit membrane.

**Figure S2.** Percentage of gold filled vessels in a transverse section of fresh and

942 dried-rehydrated petioles injected with colloidal gold particles of 5, 10, 20, and 50 nm
943 at 6 and 200 kPa.

944 **Figure S3.** Percentage of gold filled vessels in transverse sections at the distal end of
945 petioles and vessel length distribution in petioles of three species.

946 **Table 1** Summary of pore sizes in interconduit pit membranes of fresh or dried samples from various angiosperm species based on different
947 techniques reported in literature.

| Species | Sample | Pore sizes (nm) | Method | References |
|---|---|---|---|---|
| > 21 species | Dried | 39-700 | Scanning electron microscopy (SEM) observation | e.g., Sperry & Tyree (1988); Sano (2005); Jansen et al. (2009); Hillabrand et al. (2016) |
| *Rhododendron ponticum* | Dried | 82-200 | Air-injection | Crombie et al. (1985) |
| *Acacia amoena* | Fresh | < 33.3-36.8 | Paint and ink injection | Williamson & Milburn (2017) |
| *Alphitonia excelsa*, *Austromyrtus bidwillii*, *Brachychiton australis*, *Cochlospermum gillivraei*, *Drimys winteri*, *Fraxinus americana*, *Sophora japonica* | Fresh | 5-20 | Colloidal gold perfusion | Choat et al. (2003, 2004); Zhang et al. (2017) |

948

949 **Table 2** Summary of the intervessel pit membrane thickness ($T_{PM}$) and pore sizes in fresh and dried-rehydrated samples of angiosperms,
950 and the shrinkage percentage of intervessel pit membranes. Pore sizes were estimated based on the perfusion capacity of gold particles
951 with a known diameter of 5, 10, 20, and 50 nm under 6 kPa, except for values in brackets under 200 kPa. $T_{PM}$ values represent mean ± SE
952 values.

| Species | Organ | $T_{PM}$_F (nm) | $T_{PM}$_DR (nm) | Shrinkage (%) | Pore size_F (nm) | Pore size_DR (nm) |
|---|---|---|---|---|---|---|
| *Acer pseudoplatanus* L. | Petiole | 282 ± 13 | 135 ± 10* | 52.3 | < 50 | < 20 |
| *Acer pseudoplatanus* L. | Stem | 219 ± 8[#] | / | / | < 50 | / |
| *Alnus glutinosa* (L.) Gaertn. | Stem | 172 ± 6 | / | / | < 50 | / |
| *Cinnamomum camphora* (L.) J.Presl | Petiole | 686 ± 18 | 370 ± 22* | 46.1 | < 5 (< 20) | < 5 (< 5) |
| *Cinnamomum camphora* (L.) J.Presl | Stem | 599 ± 22[#] | / | / | < 20 | / |
| *Corylus avellana* L. | Stem | 285 ± 7 | 117 ± 5* | 58.8 | / | / |
| *Fagus sylvatica* L. | Stem | 247 ± 7 | 117 ± 3* | 52.8 | / | / |
| *Hibiscus schizopetalus* (Dyer) Hook.f. | Stem | 353 ± 7 | / | / | < 20 | / |

| | | | | | | |
|---|---|---|---|---|---|---|
| *Liriodendron tulipifera* L. | Stem | 280 ± 18 | 163 ± 9* | 41.7 | / | / |
| *Nerium oleander* L. | Stem | 469 ± 14 | / | / | < 20 | / |
| *Persea americana* Mill. | Petiole | 504 ± 19 | 247 ± 16* | 51.0 | < 20 (< 20) | < 5 (< 5) |
| *Persea americana* Mill. | Stem | 422 ± 15# | / | / | < 20 | / |
| *Populus tremula* L. | Stem | 274 ± 10 | 137 ± 3* | 50.2 | > 20 | / |

Note: * indicates a significant difference ($p < 0.05$) between the thickness of fresh ($T_{PM}$_F) and dried-rehydrated ($T_{PM}$_DR) pit membranes. # indicates a significant difference ($p < 0.05$) in the thickness of fresh pit membranes between petioles and stems. F = Fresh, DR = Dried-rehydrated, / = unknown.

**Table 3** Porous medium characteristics for intervessel pit membranes of seven angiosperm species. The number of fibril layers (N) and distance between layers (D) was estimated based on a shrinkage model. The porosity (ε), geodesic tortuosity (τ), and constrictivity (β) values for fresh and dried pit membranes were calculated with GeoStoch software (Mayer et al., 2004).

| Species | N | D (nm) | ε_Fresh | ε_Dried | τ_Fresh | τ_Dried | β_Fresh | β_Dried |
|---|---|---|---|---|---|---|---|---|
| *Acer pseudoplatanus* L. | 7 | 24.6 | 0.81 | 0.62 | 1.03 | 1.14 | 0.79 | 0.64 |
| *Cinnamomum camphora* (L.) J.Presl | 18 | 18.6 | 0.79 | 0.62 | 1.02 | 1.11 | 0.78 | 0.71 |
| *Corylus avellana* L. | 6 | 33.5 | 0.84 | 0.62 | 1.02 | 1.15 | 0.60 | 0.69 |
| *Fagus sylvatica* L. | 6 | 26.1 | 0.81 | 0.62 | 1.03 | 1.15 | 0.79 | 0.73 |
| *Liriodendron tulipifera* L. | 8 | 16.7 | 0.77 | 0.62 | 1.03 | 1.13 | 0.81 | 0.57 |
| *Persea americana* Mill. | 12 | 23.4 | 0.81 | 0.62 | 1.02 | 1.14 | 0.78 | 0.60 |
| *Populus tremula* L. | 7 | 22.9 | 0.80 | 0.62 | 1.03 | 1.14 | 0.78 | 0.71 |

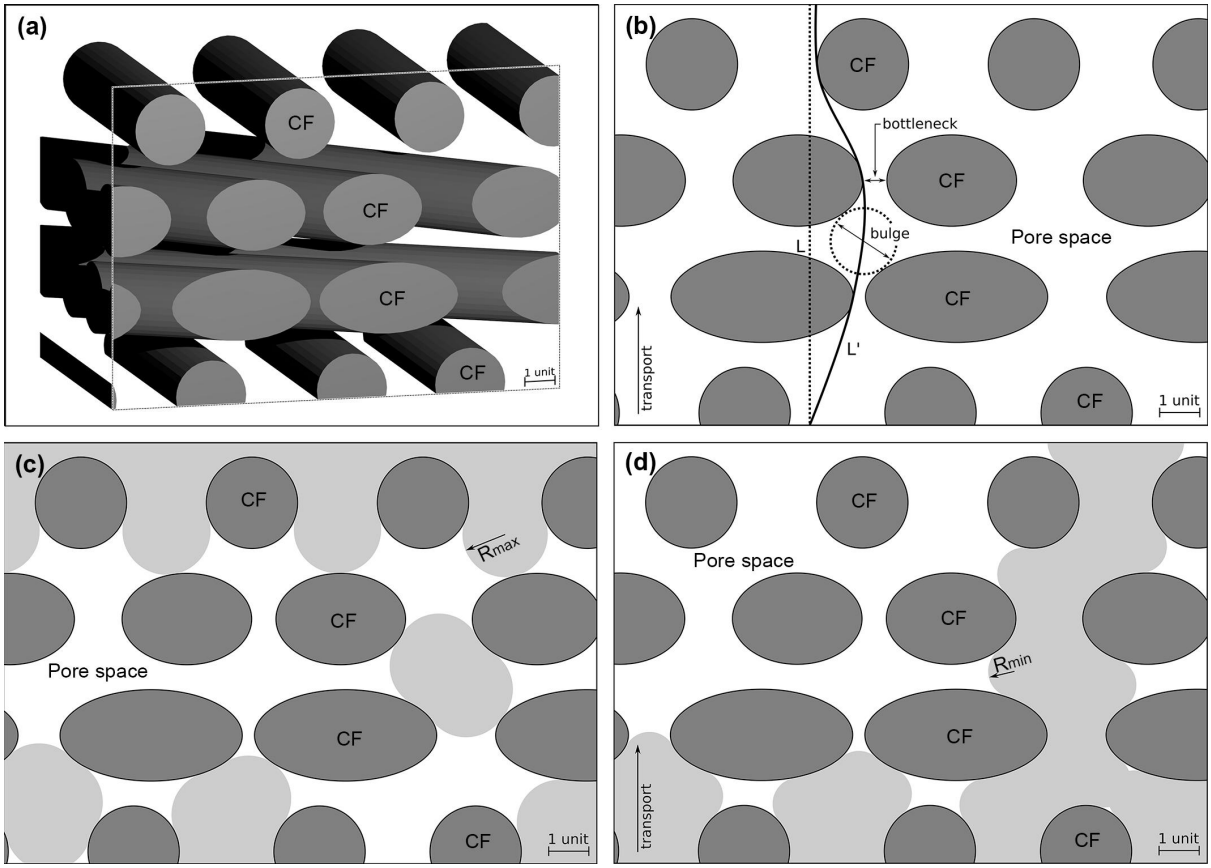


**Figure 1.** Illustration of the porous medium characteristics porosity (ε), geodesic tortuosity (τ), and constrictivity (β) in a pit membrane. A (non-orthogonal) cross section (a) from a structure similar to the three-dimensional (3D) figure (Figure S1) is used to explain three terms in 2D images. Porosity is defined as the ratio of pore volume to the total volume of the pit membrane (b). Geodesic tortuosity (b) is the ratio of the mean shortest path length of flow (L') to the thickness of the pit membrane (L). Constrictivity is traditionally defined based on the radius of (typical) bottlenecks and bulges (b). However, this definition cannot be applied to the 3D pore space in a pit membrane, which does not consist of single pores with bottlenecks and bulges. Here, constrictivity is defined based on the radii of spheres ($R_{max}$ and $R_{min}$) occupying the pore space. These spheres are allowed to overlap with each other in the

pore space, but not with the solid cellulose fibril aggregates. $R_{max}$ refers to the maximum radius of spheres covering at least 50% of pore space (c), and $R_{min}$ is the maximum radius of spheres covering at least 50% of pore space when penetrating the membrane in a certain direction (d). Dark grey circles or ellipses in b, c, and d illustrate cellulose fibril aggregates, and light grey areas in c and d represent pore space that is occupied by spheres diffusing in the pit membrane. CF = cellulose fibril aggregates.

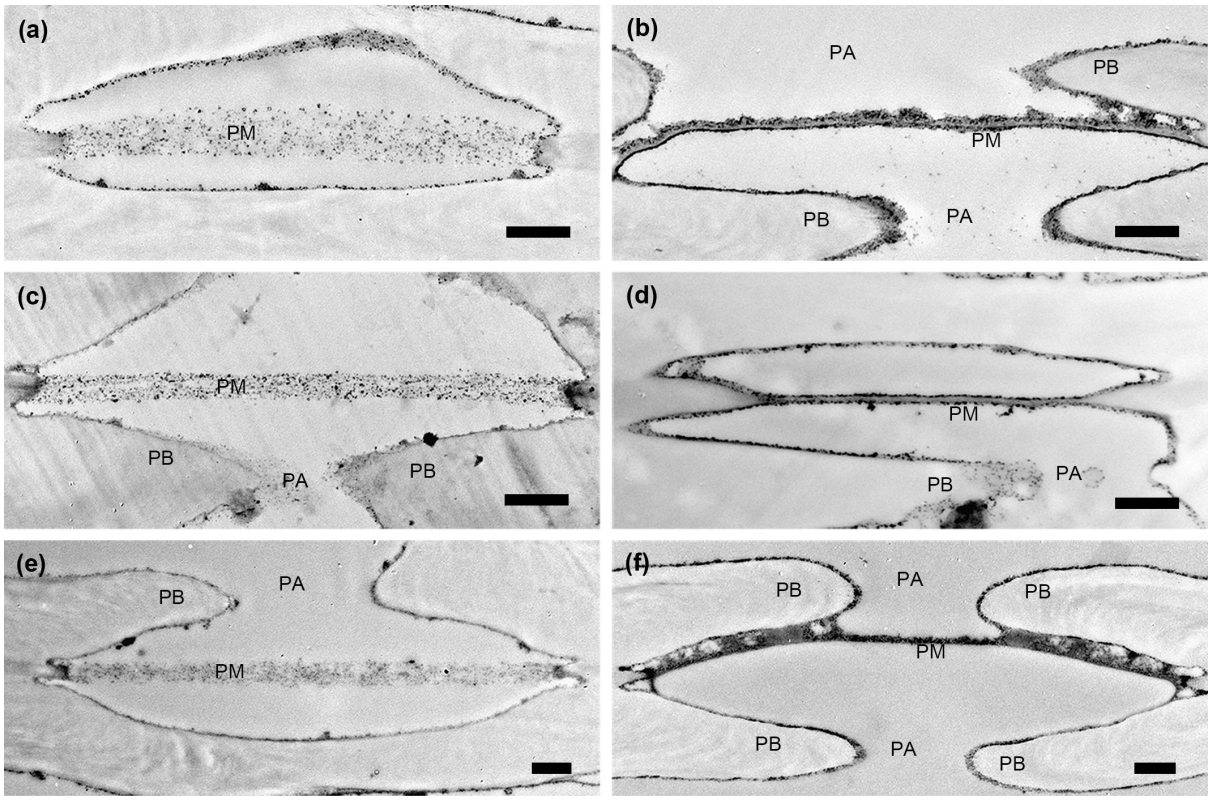


**Figure 2.** Transmission electron microscopy (TEM) images of hydrated and shrunken pit membranes in fresh (i.e., never dried prior to TEM preparation) stems of *Corylus avellana* (a, b), *Fagus sylvatica* (c, d), and *Populus tremula* (e, f). Hydrated pit membranes show an electron transparent appearance with small granular spots due to $OsO_4$ treatment. Shrunken pit membranes show a thinner thickness and darker staining, with a dark line at the outermost

983 layer of pit membranes. Aspiration occurs in some shrunken pit membranes (b, f). Pit
984 apertures are not visible in some pits because not all sections were cut through the centre of
985 the pit border (a, d, e). PA = pit aperture, PB = pit border, PM = intervessel pit membrane. All
986 scale bars = 500 nm.

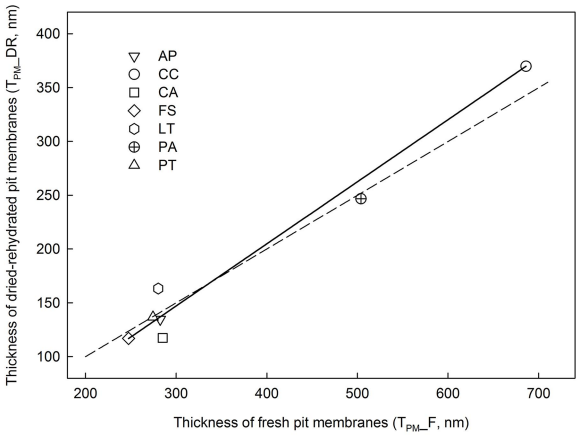


987

988 **Figure 3.** The relationship between thickness of fresh ($T_{PM}$_F) and dried-rehydrated ($T_{PM}$_DR)
989 pit membranes of seven angiosperm species as measured on transmission electron
990 microscopy (TEM) images. Data of *Acer pseudoplatanus*, *Cinnamomum camphora*, and
991 *Persea americana* were based on petioles, while the remaining four species represented stem
992 xylem. The solid line shows the fitting: $T_{PM}$_DR = 0.58$T_{PM}$_F - 25.93 ($R^2$ = 1.00, $p < 0.001$),
993 and is close to the dashed line with a slope of 0.5, which suggests a pit membrane shrinkage
994 of 50%. Data from different species were presented with different symbols. AP = *Acer*
995 *pseudoplatanus*, CC = *Cinnamomum camphora*, CA = *Corylus avellana*, FS = *Fagus*
996 *sylvatica*, LT = *Liriodendron tulipifera*, PA = *Persea americana*, PT = *Populus tremula*.

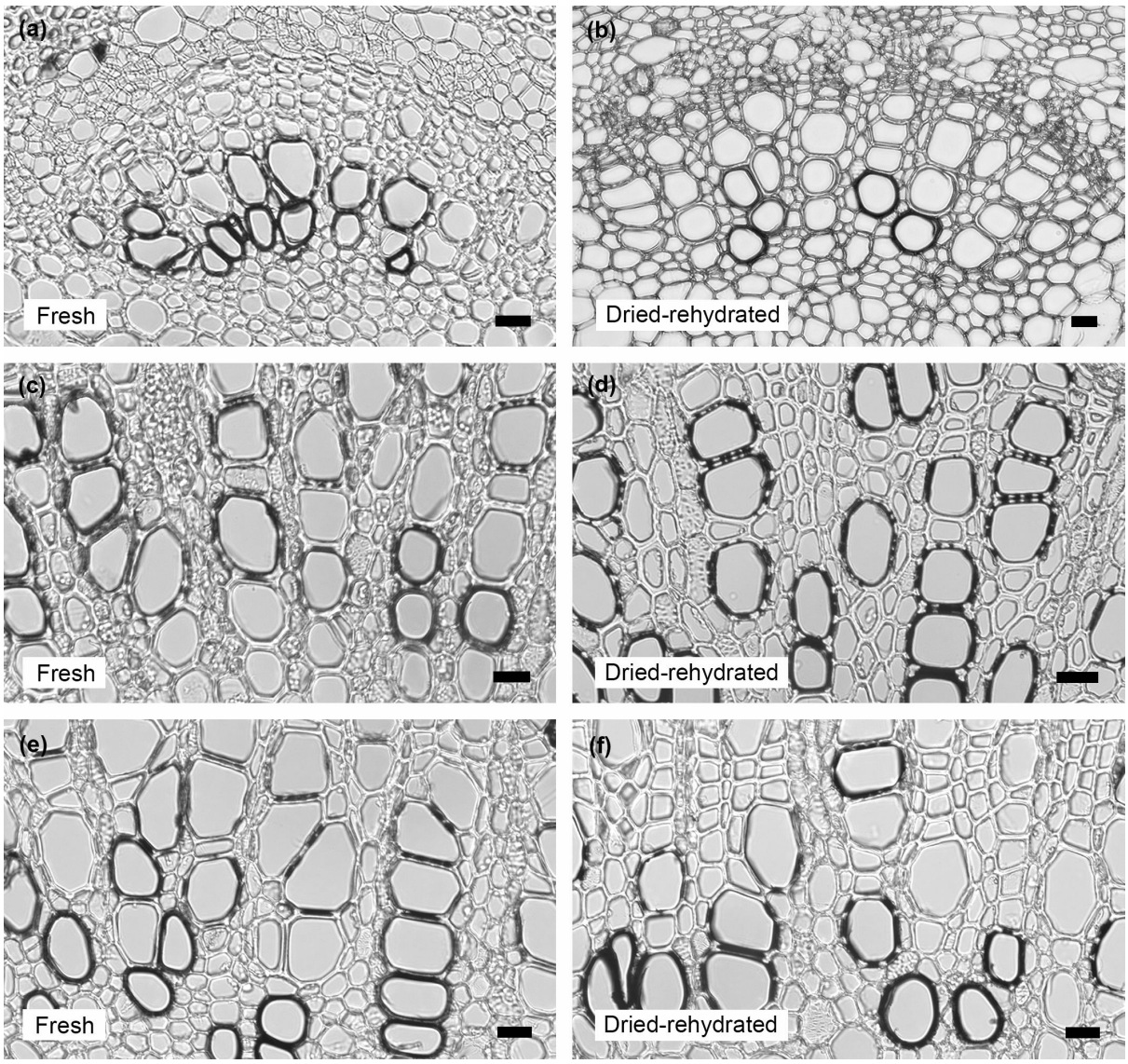


**Figure 4.** Light microscopy (LM) images of transverse sections showing xylem in fresh and dried-rehydrated petioles of *Acer pseudoplatanus* (a, b), *Cinnamomum camphora* (c, d), and *Persea americana* (e, f) injected with 5, 10, 20, and 50 nm gold particles. Sections were made at a distance of 9.5 cm, 2.5 cm, and 3.5 cm from the injection point for petioles of *A. pseudoplatanus*, *C. camphora*, and *P. americana*, respectively. Fresh and dried-rehydrated samples were cut at the same distance for three species. Petioles of *A. pseudoplatanus* were injected under 6 kPa, and petioles of *C. camphora* and *P. americana* were injected under 200

1005 kPa. The black staining in the vessel walls is the result of gold particles treated with a silver

1006 enhancer kit. All scale bars = 20 µm.

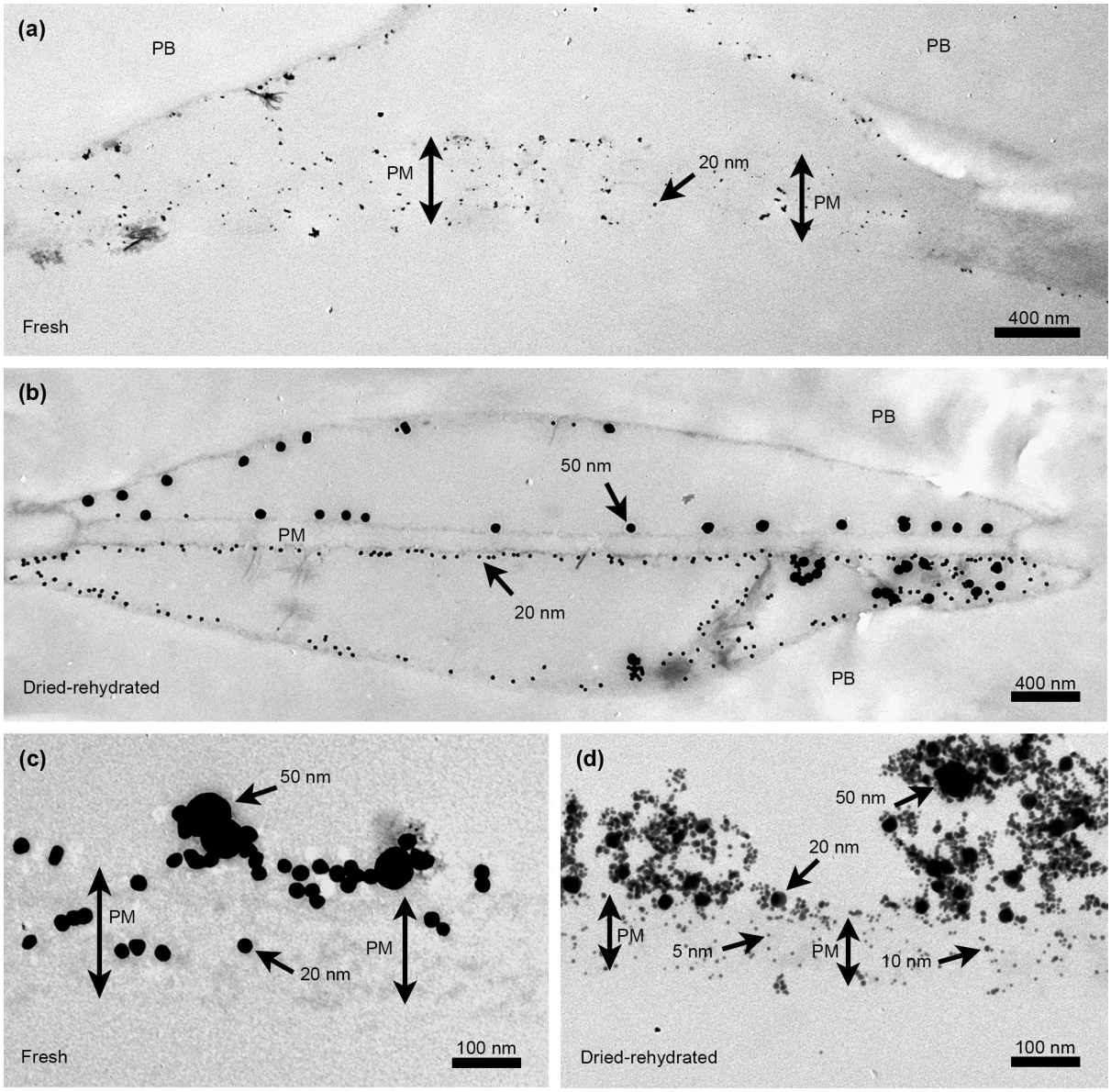


1007

1008 **Figure 5.** The distribution of gold particles in transmission electron microscopy (TEM)

1009 images of intervessel pits in xylem tissue of fresh (a, c) and dried-rehydrated (b, d) petioles of

1010 *Acer pseudoplatanus* injected with 5, 10, 20, and 50 nm gold particles under 6 kPa. Gold

1011 particles of 20 nm occur within the fresh pit membrane (a, c), and at the surface of the

1012 dried-rehydrated membrane (b, d). Besides, some irregularly shaped, grey particles clustering

1013 or coating the 20 and 50 nm gold particles (c) provides evidence for the presence of lipids
1014 associated with colloidal gold. Double arrows represent the pit membrane. Gold particles of 5,
1015 10, 20, and 50 nm are shown with black arrows. PB = pit border, PM = intervessel pit
1016 membrane.

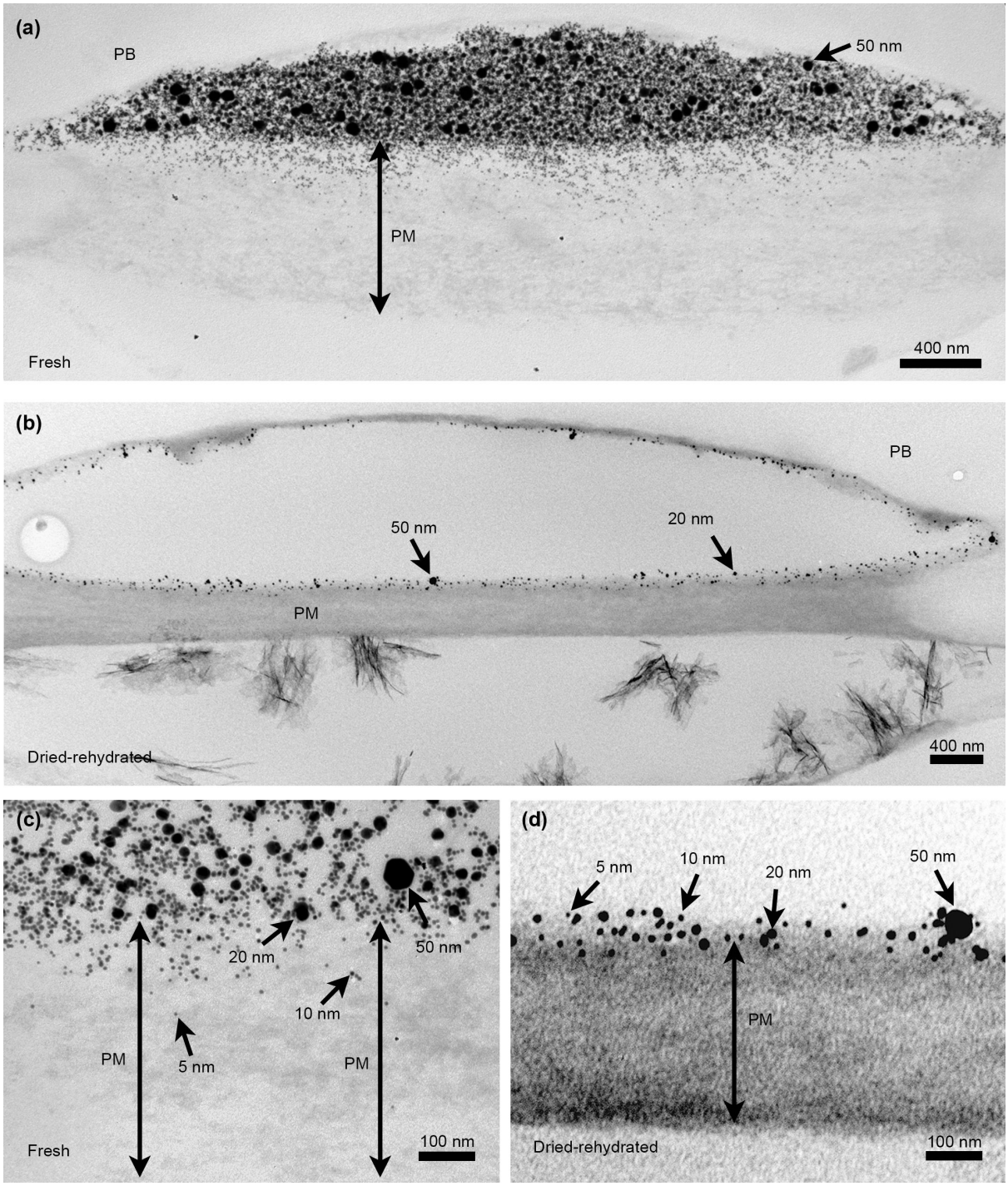


**Figure 6.** The distribution of gold particles in transmission electron microscopy (TEM) images of intervessel pits of fresh (a, c) and dried-rehydrated (b, d) petioles of *Cinnamomum camphora* injected with 5, 10, 20, and 50 nm gold particles under 200 kPa. Gold particles of 5 and 10 nm could penetrate the fresh pit membranes (c), but not the dried-rehydrated pit

membranes (d). Double arrows represent the pit membrane. Gold particles of 5, 10, 20, and 50 nm are shown with black arrows. PB = pit border, PM = intervessel pit membrane.

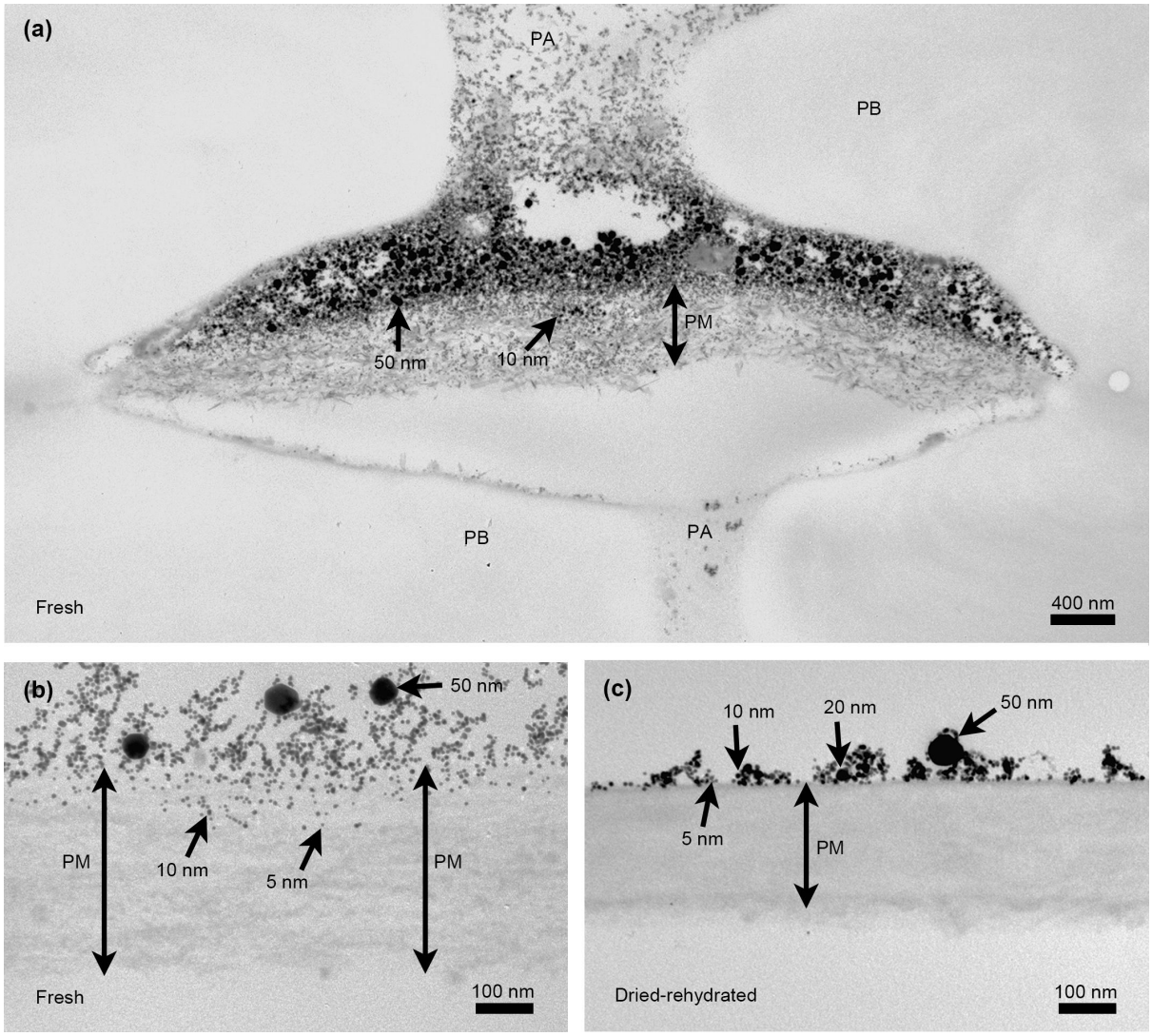


**Figure 7.** The distribution of gold particles in transmission electron microscopy (TEM) images of intervessel pits of *Persea americana* in fresh stem xylem (a), fresh xylem of a leaf petiole (b), and dried-rehydrated xylem of a leaf petiole (c). All samples were injected with 5, 10, 20, and 50 nm gold particles under 6 kPa. Gold particles of 5 and 10 nm could penetrate the fresh pit membranes (a, b), but not the dried-rehydrated pit membranes (c). Double arrows represent the pit membrane. Gold particles of 5, 10, 20, and 50 nm are shown with

black arrows. PA = pit aperture, PB = pit border, PM = intervessel pit membrane.

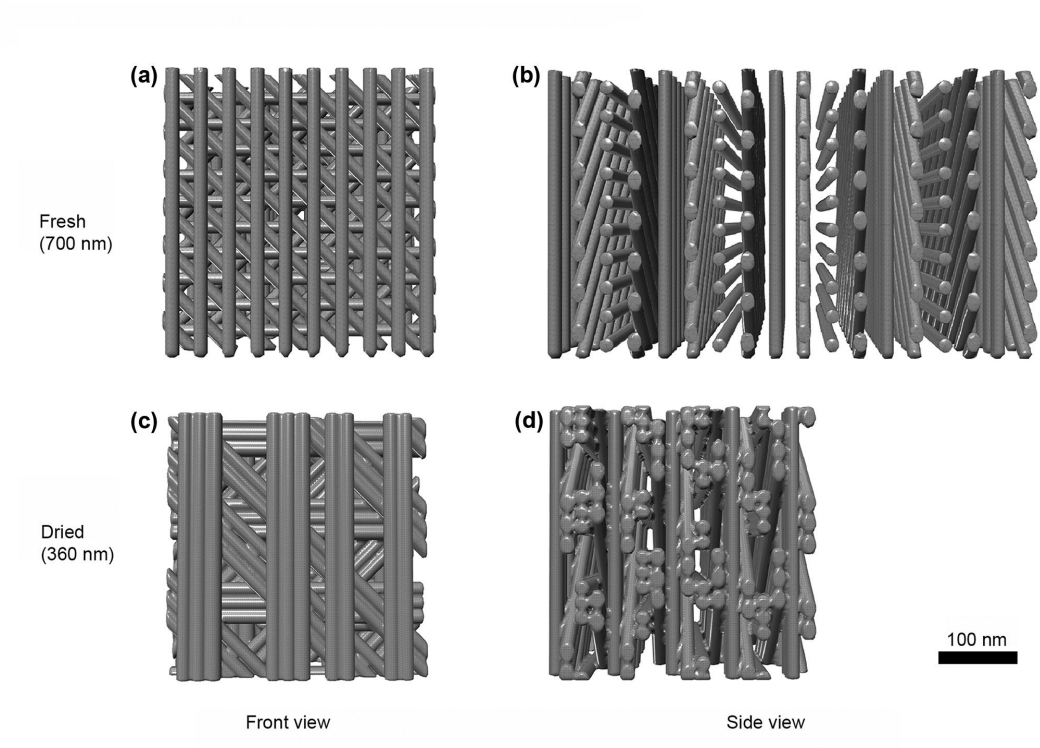


**Fig. S1** A three-dimensional (3D) intervessel pit membrane model of angiosperms showing the effect of dehydration on a pit membrane. Cellulose microfibril aggregates with a thickness of 20 nm are aligned parallel to each other within a single layer, with a 20 nm distance between each fibril (a) and each layer (b). Microfibril layers show a 45° orientation to a neighbouring layer (b). When dehydration occurs, cellulose microfibril aggregates are assumed to group randomly in pairs of 2 or 3 aggregates within a single layer (c), and the distance between layers is reduced to zero (d), which results in a 48.6% shrinkage of the pit membrane shown. The images are based on TEM observations of fresh and dried, shrunken pit membranes of *Cinnamomum camphora*.

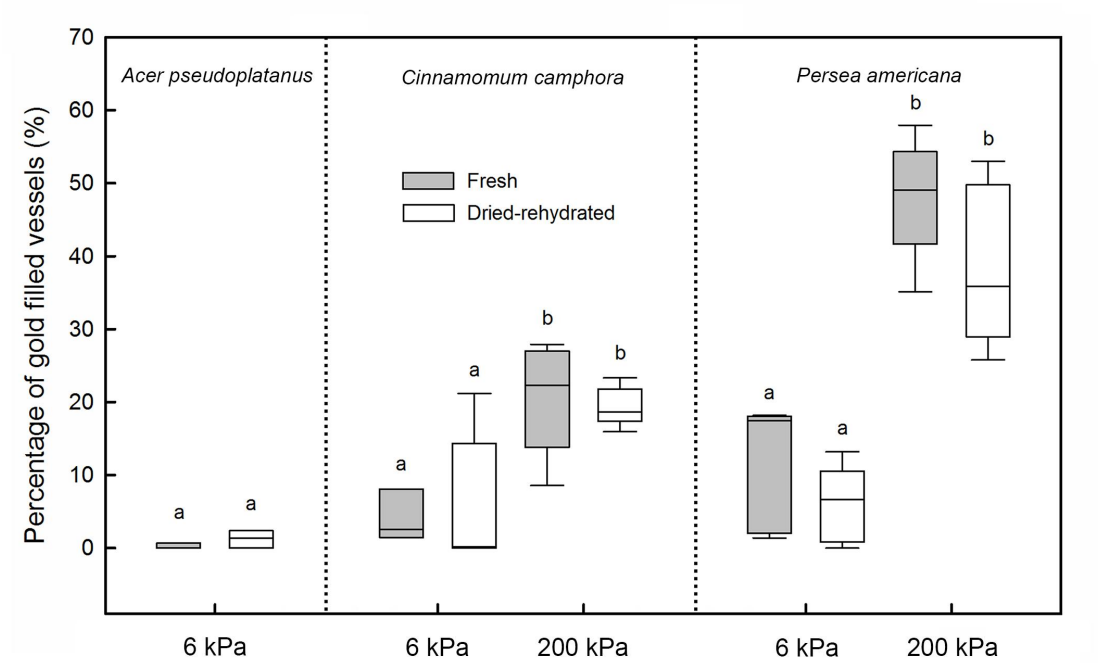


1042

1043 **Fig. S2** Percentage of gold filled vessels in transverse xylem sections of fresh and
1044 dried-rehydrated petioles of *Acer pseudoplatanus*, *Cinnamomum camphora*, and *Persea*
1045 *americana* injected with 5, 10, 20, and 50 nm gold particles under 6 and 200 kPa. Sections
1046 were made at a distance of 9.5 cm, 2.5 cm, and 3.5 cm from the injection point for petioles of
1047 *A. pseudoplatanus*, *C. camphora*, and *P. americana* respectively. Pressure of 200 kPa was not
1048 applied in petioles of *A. pseudoplatanus*. Different letters indicate significant difference.
1049 Boxes show the median, 25th, and 75th percentiles, and error bars show 10th and 90th
1050 percentiles.

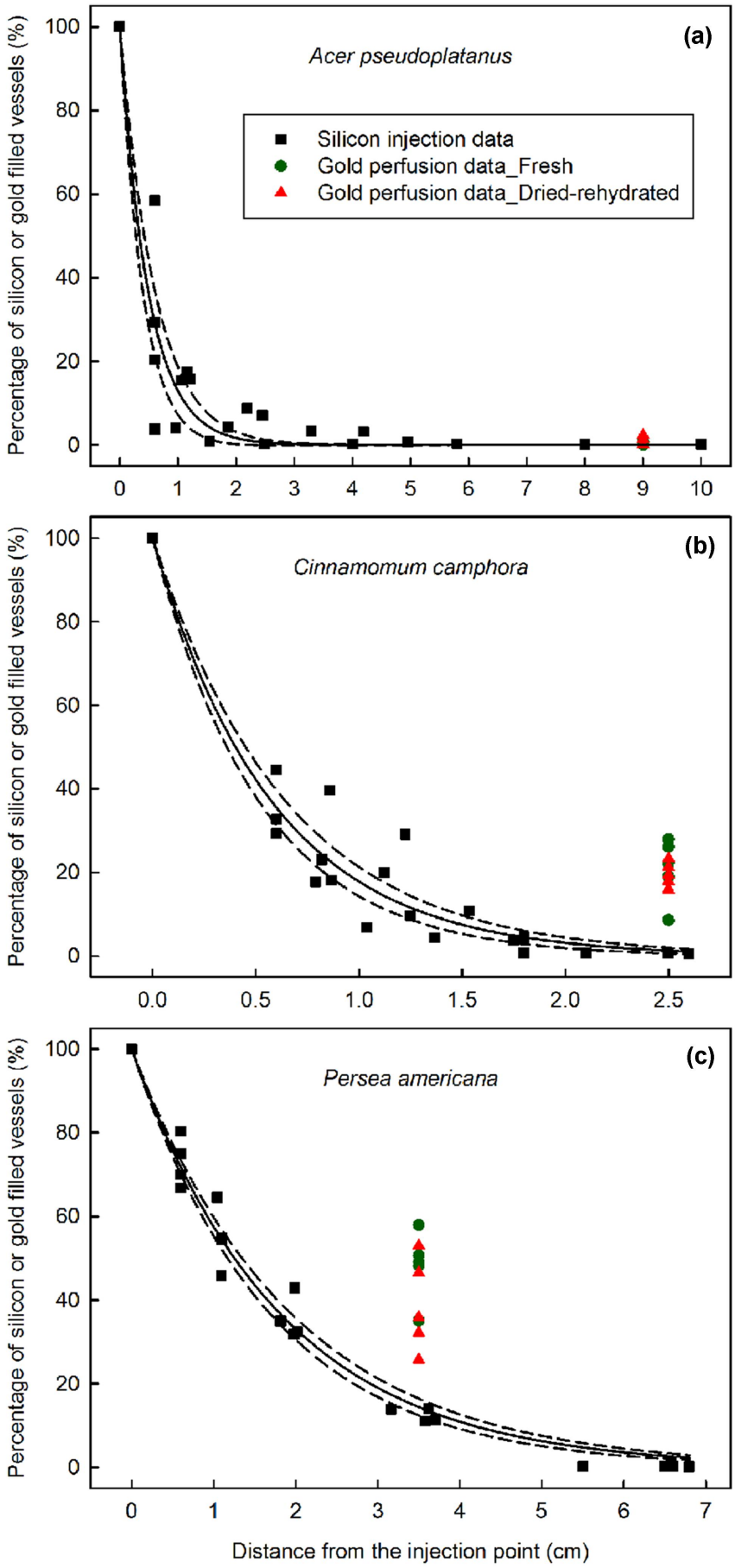
(a)
Acer pseudoplatanus
Silicon injection data
Gold perfusion data_Fresh
Gold perfusion data_Dried-rehydrated
Percentage of silicon or gold filled vessels (%)
(b)
Cinnamomum camphora
Percentage of silicon or gold filled vessels (%)
(c)
Persea americana
Percentage of silicon or gold filled vessels (%)
Distance from the injection point (cm)

1051

1052 **Fig. S3** Percentages of gold filled vessels at the distal end of petioles and vessel length
1053 distribution in petioles of *Acer pseudoplatanus* (a), *Cinnamomum camphora* (b), and *Persea*
1054 *americana* (c). Gold particles of 5, 10, 20, and 50 nm were perfused into petioles at 6 kPa for
1055 *A. pseudoplatanus*, and at 200 kPa for *C. camphora* and *P. americana*. Percentages of gold
1056 filled vessels were counted from transverse sections at a distance of 9.5 cm, 2.5 cm, and 3.5
1057 cm from the injection point for petioles of *A. pseudoplatanus*, *C. camphora*, and *P.*
1058 *americana*, respectively. Black squares represent the vessel length distribution data based on
1059 silicon injection. Solid curves show the fitting curves and dashed curves show the 95%
1060 confidence bands. Green circles and red triangles represent percentages of gold filled vessels
1061 in fresh and dried-rehydrated petioles respectively.